University of Thessaly
School of Engineering
Department of Mechanical Engineering

Diploma Thesis

Bending of Thin-Walled Elastic Beams: Analytical & Numerical Solutions

by

FILIPPOS ALEXANDRIS

Submitted in Partial Fulfilment of the
Requirements for Diploma in Mechanical Engineering
2025

Approved by the Three Members of the Advisory Committee:

First Member (Supervisor)

Professor Nikolaos Aravas
Department of Mechanical Engineering, University of Thessaly

Second Member

Assistant Professor Michalis Agoras
Department of Mechanical Engineering, University of Thessaly

Third Member

Dr. Sotiria Chouliara
Department of Mechanical Engineering, University of Thessaly

Abstract

Bending of thin-walled elastic beams: Analytical & Numerical Solutions

Filippos Alexandris

Supervisor: Professor N. Aravas

Thin-walled beams are extensively used in structural applications where material efficiency and high stiffness-to-weight ratios are critical, such as in aerospace frames, ship hulls, and lightweight civil structures. As such, prismatic thin-walled beams hold a strong position in modern engineering. In regular solid cross-section beams, classical beam theory dismisses shear stresses most of the time and mainly focuses on normal stresses since, in traditional beams, the magnitude of normal stresses is much greater. Contrary to traditional solid cross sections, in many cases thin-walled cross sections exhibit a different behavior. The order of magnitude of the shear stresses in such beams is analogous to their normal counterparts, and in some instances, may even exceed them. This thesis is focused on extracting the analytical approximate solution for the shear stresses in thin-walled beams with prismatic cross sections. The methods used for this purpose are the *Saint Venant's method* for bending of linear elastic isotropic beams, in order to set up the initial problem and extract the normal stress distribution (σ_{xx}). The extraction of the analytical solution for (σ_{xy}) and (σ_{xz}) shear stresses distribution, is made possible with the use of the *Technical Bending Theory* in conjunction with *Jourwasky's equation.* That analytical solution later on is compared to a numerical solution generated using the commercial FEA program ABAQUS.

Keywords: Technical Bending Theory; Thin-walled beam; Finite Element Method;

Acknowledgements

I would like to express my sincere gratitude to my supervisor, Professor Nikolaos Aravas, for his continuous guidance, support, and insightful feedback throughout the course of this work.

I am also thankful to postdoctoral researcher Dr. Sokratis Xenos for his support and guidance on technical subjects throughout this thesis.

Last but certainly not least, I am deeply grateful to my family for their unwavering support, patience, and belief in me during this journey.

Contents

List of Figures

List of Tables

Introduction

Thin-walled beam structures are fundamental components in various fields of engineering, particularly in aerospace, civil, and mechanical applications, where high strength-to-weight ratios are essential. These elements often exhibit complex mechanical behavior due to their geometry, especially when subjected to transverse loading. Unlike solid cross-sections, thin-walled beams can undergo significant warping and shear deformation, if the load is not carefully applied.

The classical theories of bending, such as the Euler-Bernoulli or Timoshenko beam models, often fall short in accurately describing the internal stress distribution within thin-walled open or closed cross-sections. So, to overcome these issues, the *Technical Bending Theory along* with *Jourawsky's equation* [3] are employed. Despite that, this solution is not the exact one; it offers accurate enough results on the shear stress distribution τ caused by bending. The initial problem is set up using the *Saint Venant's method* for bending, and the normal stress distribution (σ_{xx}) is part of the exact solution. For the shear stresses (σ_{xy} and σ_{xz}) though, the exact solution involves the calculation of two harmonic functions (φ_1 and φ_2), and is way more complex, [4]. So, the aforementioned combination of the Technical Bending Theory and Jourawsky's equation is used to extract accurate analytical results.

Regarding numerical approximations, the Finite Element Method has proven itself in the field of solid mechanics, providing excellent numerical approximations in stress and strain fields - if the FE model is well established. Like in any other scenario, a thin-walled beam can be modeled in any commercial FEA software. In this thesis, all thin-walled beams have been modeled and analyzed using the commercial FEA software ABAQUS.

In chapter 1, the theory behind the bending of thin-walled beams with a transverse load is presented, along with the aforementioned analytical solutions for each type of beam, whether it is a beam with an open or closed cross-section. Chapter 2 includes two main concepts, the first one involves the generation of the shell's two-dimensional profile in ABAQUS CAE and its subsequent exporting in the 3rd dimension. The second concept is fairly simple, being the comparison between the numerical solution derived by ABAQUS to the analytical one extracted in the first chapter.

Chapter 1

Bending With Transverse Load of Thin Walled Beams

1.1 Bending and Torsion of Thin Walled Beams

In this section, follows a presentation of the coordinate systems used to aid in the analysis of thin-walled beams, along with the definition of the initial problem based on Saint Venant's method for bending of beams with a transverse load.

1.1.1 Coordinate Systems

In order to properly analyze thin-walled beams, two separate coordinate systems are established. Thin-walled beams have two major characteristic traits. The first one is referred to as the "mid line", denoted as C. The mid-line is an imaginary line running across the middle of the cross-section, splitting it into two equal halves. The second trait is the thickness of the cross-section, $t(s)$. Let s be the arc length through C, see figure (1.1). In this thesis, the thickness $t(s)$ is considered to be constant all through the beam. These two coordinate systems are presented below.
The first coordinate system (x, y, z), is **Cartesian** right hand, central, and principal, i.e., such that

$$\int_\Omega y\, dA = \int_\Omega z\, dA = 0 \qquad \text{and} \qquad I_{yz} = -\int_\Omega y\, z\, dA = 0.$$

The x-direction is along the axis of the beam (parallel to the traction-free lateral surface), and the unit vectors along the coordinate axes are denoted by $(\mathbf{e}_x, \mathbf{e}_y, \mathbf{e}_z)$. The length of the beam is ℓ with its bases at $x = 0$ and $x = \ell$.

Regarding the second coordinate system, a cross-sectional point of view is adopted, and a curvilinear coordinate system (x, n, s) is utilized (see Figure 1.1). The x coordinate remains the same in both systems (axial coordinate). The coordinate s is measured along the length of the mid-line C, and the coordinate n is perpendicular to s (i.e., perpendicular to the mid-line).

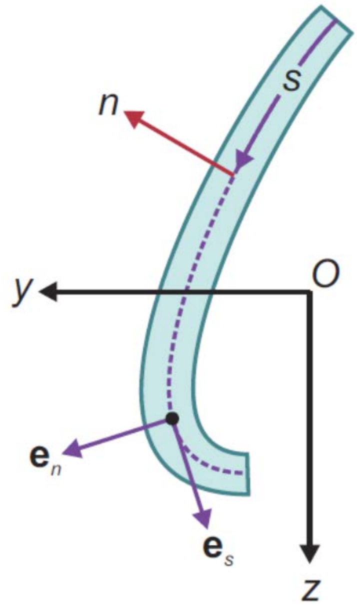

Figure 1.1: Random thin-walled cross-section. The curvilinear coordinates (s, n) are presented along with the respective unit vectors (e_s, e_n), (adapted from [3]).

In terms of dimensions, s varies between $0 \leq s \leq L_C$, and n varies between $-t(s)/2 \leq n \leq t(s)/2$.

Similar to the Cartesian coordinate system, the unit vectors $\mathbf{e}_s(s)$ and $\mathbf{e}_n(s)$ are defined such that $\mathbf{e}_s(s)$ is tangent to C, and $\mathbf{e}_n(s) = \mathbf{e}_s(s) \times \mathbf{e}_x$ is normal to C (see Figure 1.1).

These two coordinate systems are used throughout this thesis to extract all stress distributions.

1.1.2 Bending With Transverse Load

Saint Venant's beam theory is utilized in this section to examine the problem of a thin-walled beam bending under transverse loading. The material of the beam is considered to be linear elastic, isotropic and homogeneous, and is described by two constants: the Young's modulus E and Poisson's ratio ν.

Both the Cartesian (x, y, z) and the curvilinear (x, n, s) coordinate systems used in this analysis have been introduced in the previous subsection.

The beam is loaded at the $x = \ell$ base, with a transverse load

$$\mathbf{R}^\ell = Q_y\,\mathbf{e}_y + Q_z\,\mathbf{e}_z,$$

applied at the point $(x, y, z) = (\ell, y_0, z_0)$.

The $x = 0$ base of the beam is fixed, meaning:

$$\mathbf{u}^0 = 0,$$

i.e., all displacements and rotations are constrained at that base. To maintain static equilibrium, necessary support reactions and moments are applied at $x = 0$ beam base. The lateral surface of the beam remains unloaded, and all body forces are neglected ($\mathbf{b} = 0$). At any cross section, the total transverse load vector is:

$$\mathbf{Q} = Q_y \, \mathbf{e}_y + Q_z \ , \mathbf{e}_z = \text{Constant}. \tag{1.1}$$

Similarly, the total moment vector at any section is:

$$\mathbf{M}(x) = (\ell - x)(-Q_z \, \mathbf{e}_y + Q_y \, \mathbf{e}_z) + (y_0 \, Q_z - z_0 \, Q_y)\mathbf{e}_x \equiv M_y(x) \, \mathbf{e}_y + M_z(x) \, \mathbf{e}_z + T^Q \, \mathbf{e}_x. \tag{1.2}$$

Note:

- The beam is not subjected to axial loading.
- The torsional moment component $T_Q \equiv y_0 \, Q_z - z_0 \, Q_y$ is constant and originates from the eccentric placement of the transverse load $\mathbf{R}^\ell$.

The normal stress distribution based on the **exact** solution [4] is given by:

$$\sigma_{xx}(x, y, z) = \frac{M_z(x)}{I_y} z - \frac{M_y(x)}{I_z} y, \tag{1.3}$$

where

$$M_y(x) = -(\ell - x)Q_z, \quad M_z(x) = -(\ell - x)Q_y, \tag{1.4}$$

and (I_y, I_z) are the beam's principal moments of inertia. Using (1.3) to derive

$$\frac{\partial \sigma_{xx}}{\partial x} = \frac{Q_z}{I_y} z + \frac{Q_y}{I_z} y. \tag{1.5}$$

The exact solution for the shear stress distribution is way more complex and involves the calculation of two harmonic functions φ_1 & φ_2 [4].

In the following sections, a relatively simple but accurate methodology is used to calculate the shear stresses in thin-walled beams. That methodology is based upon the Jourawsky's equation [3].

1.2 Open Thin-Walled Sections

An open section is illustrated in Figure 1.2. According to the exact solution [3], the stress tensor in the *Cartesian* and *Curvilinear* coordinate systems takes the following form:

$$\boldsymbol{\sigma}_{Cartesian} = \begin{bmatrix} \sigma_{xx} & \sigma_{xy} & \sigma_{xz} \\ \sigma_{xy} & 0 & 0 \\ \sigma_{xz} & 0 & 0 \end{bmatrix}, \qquad \boldsymbol{\sigma}_{Curvilinear} = \begin{bmatrix} \sigma_{xx} & \sigma_{xs} & \sigma_{xn} \\ \sigma_{xs} & 0 & 0 \\ \sigma_{xn} & 0 & 0 \end{bmatrix}.$$

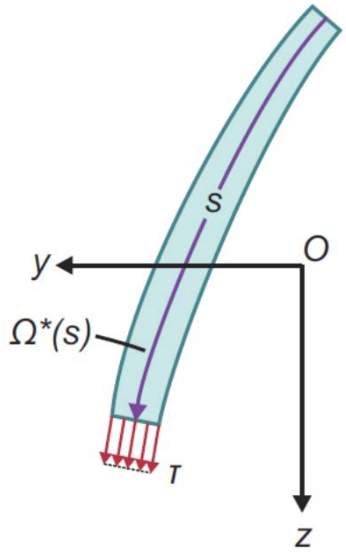

Figure 1.2: Shear stress distribution in random open thin-walled cross-section (adapted from [3]).

To simplify the analysis, $\sigma_{xz} = \sigma_{xn} \simeq 0$ is assumed. This assumption is based upon the fact that the thickness of the beam is a very small quantity compared to the rest dimensions. Thus, there is not sufficient physical space for the aforementioned shear stresses to develop. Thus, the total shear stress across the beam is always parallel to the mid-line C. Hence, the total stress vector can be written as:

$$\mathbf{t} = \sigma_{xx}\,\mathbf{e}_x + \tau\,\mathbf{e}_s, \quad \text{where} \quad \tau \equiv \sigma_{xs}.$$

Shear stress (τ) calculations are based upon the Technical Bending Theory and Jourawski's equation; as such, the enhanced shear stresses are calculated.

Considering a random cross section that is part of an open thin-walled section, let the area of that section be denoted as $\Omega^*(s)$ as illustrated in Figure 1.2. According to [3], the mean value of the shear stress τ across the thickness at position s is given by

$$\bar{\tau}(s) = -\frac{1}{t(s)}\int_{\Omega^*(s)} \frac{\partial \sigma_{xx}}{\partial x}\,dA = -\frac{1}{t(s)}\int_{\Omega^*(s)} \left(\frac{Q_z}{I_y}z + \frac{Q_y}{I_z}y\right)\,dA, \tag{1.6}$$

where $\partial\sigma_{xx}/\partial x$ was acquired from (1.5)

As mentioned previously, the thickness of the beam is significantly smaller than the rest of the dimensions; as such, τ is assumed to remain constant through the thickness. So, $\tau(n,s) \cong \tau(s) = \bar{\tau}(s)$, and the area integral now may be computed disregarding all functions related to t. Using all corresponding mid-line parameters, the last equation takes the following form

$$\tau(s) \cong -\frac{1}{t(s)}\int_0^s \left[\frac{Q_z}{I_y}z(s') + \frac{Q_y}{I_z}y(s')\right]\,t(s')ds',$$

which it equivalent to

$$\boxed{\tau(s) = -\frac{1}{t(s)}\left[\frac{Q_z}{I_y}S_y^*(s) + \frac{Q_y}{I_z}S_z^*(s)\right]}, \tag{1.7}$$

where

$$\boxed{S_y^*(s) = \int_0^s z(s')t(s')ds'} \qquad \text{and} \qquad \boxed{S_z^*(s) = \int_0^s y(s')t(s')ds'}. \tag{1.8}$$

The quantities above are area's $\Omega^*(s)$ static moments of inertia with respect to the central principal coordinate axes y and z of the cross section.

Total transverse load & torsional moment caused by the shear stresses distribution (1.7)

The following formulas are used to calculate the total transverse load & torsional moment due to the shear stress distribution (1.7). These relations are presented in greater depth and subsequently proven in [3].

$$\int_C S_y^*(s)\,dz(s) = -I_y, \qquad \int_C S_z^*(s)\,dy(s) = 0, \tag{1.9}$$

$$\int_C S_z^*(s)\,dy(s) = -I_z, \qquad \int_C S_z^*(s)\,dz(s) = 0, \tag{1.10}$$

and

$$\int_C S_y^*(s)\,r_n(s)\,ds = -\int_C \omega(s)\,z(s)\,t(s)\,ds, \tag{1.11}$$

$$\int_C S_z^*(s)\,r_n(s)\,ds = -\int_C \omega(s)\,y(s)\,t(s)\,ds, \tag{1.12}$$

where, $r_n(s)$ is the perpendicular distance between the tangent to the mid-line C and the cross section's geometric center O, (see figure 1.3), and $\omega(s)$ is the sectoral surface, (see figure 1.4).
To proceed with the calculations, a relation between ds, dz and dy is needed. So, let $\theta(s)$ be the angle between the mid-line's C tangent and central & principal z axis. Thus,

$$\sin\theta(s) = \frac{dy(s)}{ds} \qquad \text{and} \qquad \cos\theta(s) = \frac{dz(s)}{ds},$$

$y(s)$ and $z(s)$ are the coordinates of a random mid-line C point. The total force in the z direction due to shear stress distribution $\tau(s)$, (eq. (1.7)) is computed by

$$F_z^\tau \equiv \int_0^{L_C} \tau(s)\underbrace{\cos\theta(s)}_{dz(s)/ds}\,t(s)\,ds = \int_{s=0}^{L_C} \tau(s)\,t(s)\,dz(s),$$

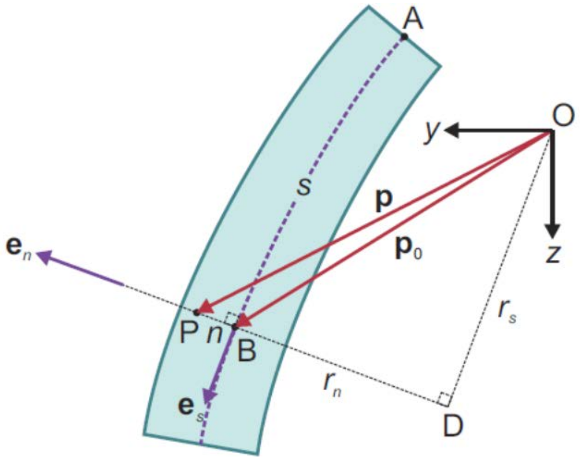

Figure 1.3: $\vec{OP} = \mathbf{p}, \vec{OB} = p_0, OD = r_s, DB = r_n, \hat{AB} = s, BP = n$ (adapted from [3]).

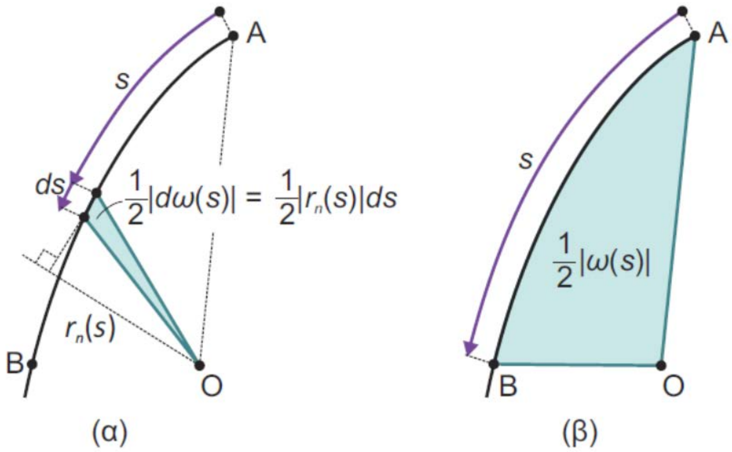

Figure 1.4: The sectoral surface $\omega(s) = \int_0^s r_n ds$ across the mid-line C of the cross-section (adapted from [3]).

where L_C is the mid-line's length. Substituting $\tau(s)$ from (1.7) leads to

$$F_z^\tau = -\int_{s=0}^{L_C} \left[\frac{Q_z}{I_y} S_y^*(s) + \frac{Q_y}{I_z} S_z^*(s)\right] dz(s) = $$
$$= -\frac{Q_z}{I_y} \underbrace{\int_{s=0}^{L_C} S_y^*(s)\, dz(s)}_{=-I_y} - \frac{Q_y}{I_z} \underbrace{\int_{s=0}^{L_C} S_z^*(s)\, dz(s)}_{=0} = Q_z, \tag{1.13}$$

reaching this conclusion involved the utilization of (1.9) & (1.10) relations. Similarly, it is concluded that for the y direction the total force attributed to shear stress $\tau(s)$ distribution is equivalent to $F_y^\tau \equiv \int_0^{L_C} \tau(s) \sin\theta(s) t(s) ds = Q_y$. These results point out that shear stress distribution τ is in context with the applied transverse forces (Q_y,Q_z). Next, the torsional moment about the central & principal x axis is calculated;

$$T^{\tau} \equiv \int_C \tau(s) r_n(s) t(s) ds, \tag{1.14}$$

T^{τ} torsional moment is the result of shear stress τ distribution as well.

Substituting relation (1.7) to (1.14) yields

$$T^{\tau} = -\frac{Q_z}{I_y} \int_0^{L_C} S_y^*(s) r_n(s) ds - \frac{Q_y}{I_z} \int_0^{L_C} S_z^*(s) r_n(s) ds.$$

A final substitution of (1.11) and (1.12) to the relation above leads to

$$T^{\tau} = Q_z \, y_s - Q_y \, z_s,$$

where

$$y_s = \frac{1}{I_y} \int_o^{L_C} z(s) \omega(s) t(s) ds, \quad z_s = -\frac{1}{I_z} \int_o^{L_C} y(s) \omega(s) t(s) ds.$$

Coordinates y_s and z_s solely depend on the cross section's geometry and define the *shear center* of the thin-walled beam.

Shear Center

The torsional moment T^Q about x axis due to transverse forces equates to

$$T^Q = Q_z \, y_0 - Q_y \, z_0.$$

In order for the shear stress distribution τ to be in context with the applied transverse forces (Q_y,Q_z),

$$\boxed{T^{\tau} = T^Q \quad \forall \; (Q_y, Q_z)}, \tag{1.15}$$

meaning

$$(y_0 - y_s) Q_z - (z_0 - z_s) Q_y = 0 \quad \forall \; (Q_y, Q_z).$$

From the last relation, it is concluded that in order for the shear stress τ formula (1.7) to hold true, (y_0, z_0), the coordinates of the load application point $\mathbf{R}^{\ell} = Q_y \, \mathbf{e}_y + Q_z \, \mathbf{e}_z$ at the $x = \ell$ base of the beam, should be equivalent to

$$\boxed{y_0 = y_s \equiv \frac{1}{I_y} \int_0^{L_C} \omega(s) z(s) t(s) ds} \quad \text{and} \quad \boxed{z_0 = z_s \equiv -\frac{1}{I_y} \int_0^{L_C} \omega(s) y(s) t(s) ds}. \tag{1.16}$$

The above mentioned equations define the shear center of the thin walled cross section, in regard to a central & principal coordinate system.

Key Notes:

- In case the transverse load $\mathbf{R}^\ell = Q_y\,\mathbf{e}_y + Q_z\,\mathbf{e}_z$ is applied to a point $(\ell,\, y_0,\, z_0)$ other than the shear center, a standard practice involves transferring $\mathbf{R}^\ell$ at the shear center of the cross section, while simultaneously considering the torsional moment $T = Q_z(y_0 - y_s) - Q_y(z_0 - z_s)$. In this case the main solution is comprised of two separate solutions;

  i. Bending with transverse load $\mathbf{R}^\ell$ placed at the cross section shear center & at the $x = \ell$ base of the beam.

  ii. Torsion with the torsional moment $T = Q_z(y_0 - y_s) - Q_y(z_0 - z_s)$.
  The shear stresses caused by T are described by the following formula;
  $\tau^T(n) = \frac{2T}{J}n$, where $J = \frac{1}{3}\int_0^{L_C} t^3(s)ds$, is the cross section's torsional constant, and $n \in \left[-\frac{t(s)}{2}, \frac{t(s)}{2}\right]$. Regarding the moment sign convention, the right hand rule applies.

- The 'classic' method for computing the shear center in thin-walled cross sections can be divided in three steps;

  i. Calculate shear stress distribution $\tau(s)$ from (1.7) relation.

  ii. Calculate T^τ from (1.14) relation.

  iii. Request $T^\tau = T^Q = Q_z\,y_0 - Q_y\,z_0$ for random (Q_y, Q_z) values and thus, solving for (y_0, z_0).

- The relation between normal stress σ_{xx} and shear stress $\tau(s)$ and more specifically the ratio $r = \sigma_{xx}/\tau(s)$, solely depends on the placement of the transverse load $\mathbf{R}^\ell$. In case the $\mathbf{R}^\ell$ is placed far from the shear center of the thin-walled beam, r may exceed unity. In contrast, most of the times classical beam theory ignores shear stresses all together, due to the fact that normal stresses (σ_{xx}), tend to be orders of magnitude larger than shear stresses in regular beams.

1.2.1 Solution for C-shell beam

Consider a regular prismatic C-channel thin-walled beam. The web of the beam is denoted as H and the flanges as $h_1 = h_2 = h$. The thickness of the cross-section is $t =$ constant, and it is significantly smaller than the web H, which is the 'characteristic' dimension of the beam. For thin-walled beam analysis, the length of the beam, ℓ, is chosen to be approximately $\ell = 10\,H$. The beam is loaded with a transverse force Q_z acting upon the $x = \ell$ beam end, Q_z is applied at a distance y_0 from the web, as illustrated in figure 1.5. Following are the calculations of the shear center y_s, shear and normal stress distributions respectively, throughout the beam.
Moving forward, the 'classic' way of calculating the shear center is used, where the shear stresses due to the transverse load are first calculated, then the torsion equation (1.14) is employed.

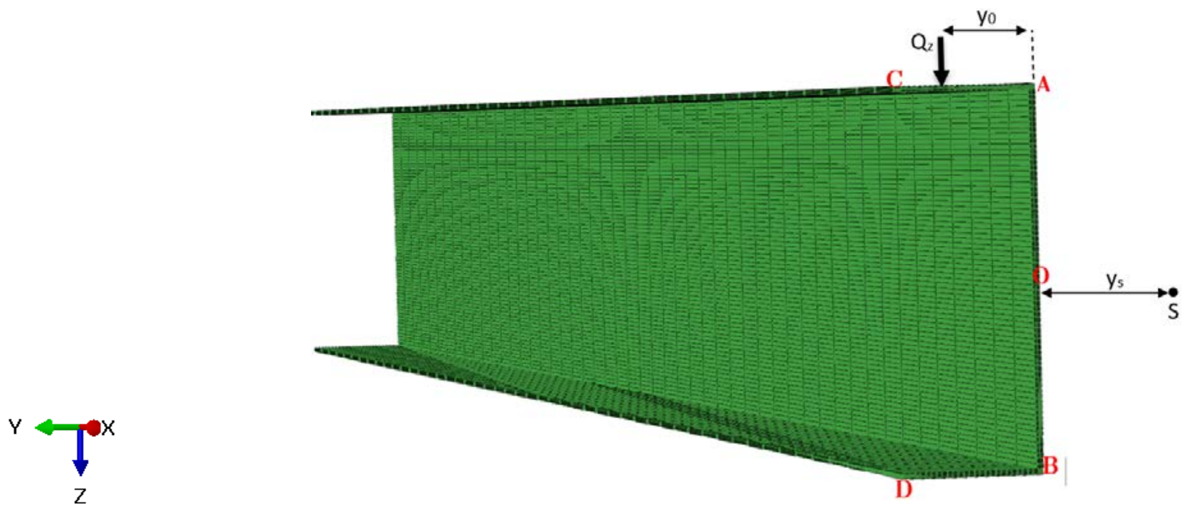

Figure 1.5: C-shell; Bending with transverse load of an open thin-walled cross section.

A non-central y-z coordinate system is used. The y axis is a symmetry axis while the z axis is non-central.

Shear stresses caused by Q_z are calculated by (1.7)

$$\tau^Q(s) = -\frac{1}{t}\frac{Q_z}{I_y}S_y^*(s).$$

Area moment of inertia I_y may be calculated in two main ways:

1. The Steiner theorem
2. $I_y = \int\limits_C z^2(s)t(s)ds$

The end result is the same,

$$I_y = \frac{1}{12}t\,H^3 + \frac{1}{6}h\,t^3 + \frac{1}{2}h\,t\,H^2$$

and $S_y^*(s)$ is calculated by

$$\begin{aligned} S_y^*(s) &= \int\limits_0^s z(s)t(s)ds = \underbrace{t\int\limits_0^{s_1}\left(\frac{H}{2} - s_1\right)ds_1}_{Web} + \underbrace{t\int\limits_0^{s_2}\frac{H}{2}ds_2}_{upper\,flange} - \underbrace{t\int\limits_0^{s_3}\frac{H}{2}ds_3}_{Lower\,flange} = \\ &= t\left(\frac{H}{2}s_1 - \frac{s_1^2}{2} + \frac{H}{2}s_2 - \frac{H}{2}s_3\right), \end{aligned} \tag{1.17}$$

where s_1, s_2 and s_3 are the curvilinear coordinates for all three branches of the cross section.

Thus, $\tau^Q(s)$ becomes

$$\tau^Q(s) = \underbrace{-\frac{Q_z}{I_y}\left(\frac{H}{2}s_1 - \frac{s_1^2}{2}\right)}_{Web} \underbrace{-\frac{Q_z}{I_y}\left(\frac{H}{2}s_2\right)}_{upper flange} \underbrace{+\frac{Q_z}{I_y}\left(\frac{H}{2}s_3\right)}_{Lower flange}, \qquad s_1 \in [0,H], \quad s_2, s_3 \in [0,h],$$

where I_y is left as is for aesthetic and practical purposes.

Next, the torsional moment about the non-central x axis caused by $\tau^Q(s)$ is calculated.[1]

$$T^\tau = \int_C \tau(s) r_n(s) t(s) ds = -\frac{Q_z}{I_y}\frac{H}{2}t\int_0^{s_2} s_2\, r_n(s_2) ds_2 + \frac{Q_z}{I_y}\frac{H}{2}t\int_0^{s_3} s_3\, r_n(s_3) ds_3 = -\frac{Q_z\, H^2\, h^2\, t}{4\, I_y}.$$

In case the transverse force acts upon the shear center y_s, the torsional moment T^Q is equivalent to $T^Q = Q_z y_s$. Thus, from (1.14) $T^\tau = T^Q$ which leads to

$$y_s = -\frac{H^2\, h^2}{4\, I_y} t.$$

The negative sign (-) indicates that the shear center lies ‘outside of the cross-section’, (see figure 1.5).

In case Q_z is not applied at the shear center ($y_0 \neq y_s$), there are additional shear stresses τ^T caused by the torsion of the beam. As mentioned in the chapter above, consider the torsional moment $T = -(y_s - y_0)Q_z$ this moment causes the aforementioned shear stresses, which are described by the following relation

$$\tau^T(n) = \frac{2\,T}{J}n, \quad -\frac{t}{2} \leq n \leq \frac{t}{2}$$

and

$$J = \frac{1}{3}\int_0^{L_C} t(s)^3\, ds = \frac{1}{3}\int_0^{H} t^3\, ds_1 + \frac{2}{3}\int_0^{h} t^3\, ds_2 = \frac{t^3}{3}(H + 2\,h),$$

thus,

$$\tau^T(n) = -\frac{6(y_s - y_0)Q_z}{t^3(H + 2\,h)}n \qquad y_s = -\frac{H^2\, h^2}{4\, I_y}t, \quad -\frac{t}{2} \leq n \leq \frac{t}{2},$$

where, J is the cross section’s torsional constant and n is the distance between the mid-line and the outer surface of the beam.

[1] Shear stress τ^Q_{AB} found in the web, does not contribute to the moment equation about the x axis.

The total shear stresses in the cross section are simply the sum of $\tau^Q(s)$ and $\tau^T(n)$

$$\boxed{\tau(s,n) = \tau^Q(s) + \tau^T(n) = \underbrace{-\frac{Q_z}{I_y}\left(\frac{H}{2}s_1 - \frac{s_1^2}{2}\right)}_{Web} \underbrace{-\frac{Q_z}{2\,I_y}H\,s_2}_{upper flange} \underbrace{+\frac{Q_z}{2\,I_y}H\,s_3}_{Lower flange} \underbrace{-\frac{6(y_s-y_0)Q_z}{(H+2\,h)t^3}n}_{\text{Everywhere}}},$$

where

$$s_1 \in [0,H], \quad s_2, s_3 \in [0,h] \quad \text{and} \quad n \in \left[-\frac{t}{2}, \frac{t}{2}\right].$$

Maximum shear stress distribution in each branch:

i. Web - AB branch
here the maximum shear stress develops at $(s_1 = \frac{H}{2}, n = \frac{t}{2})$ and takes the value

$$|\tau^{AB}|_{\max} = \frac{Q_z}{I_y}\frac{H^2}{8} + \frac{3(y_s-y_0)Q_z}{(H+2\,h)t^2}.$$

ii. Upper flange - AC section
here the maximum shear stress develops at $(s_2 = h, n = \frac{t}{2})$ and takes the value

$$|\tau^{AC}|_{\max} = \frac{Q_z}{I_y}\frac{H\,h}{2} + \frac{3(y_s-y_0)Q_z}{(H+2h)t^2}.$$

iii. Lower flange - BD section
here the maximum shear stress develops at $(s_3 = h, n = -\frac{t}{2})$ and takes the value

$$|\tau^{BD}|_{\max} = \frac{Q_z}{I_y}\frac{H\,h}{2} + \frac{3(y_s-y_0)Q_z}{(H+2\,h)t^2}.$$

Normal stress distribution

The bending moment distribution across the beam is

$$M(x) = -Q_z(\ell - x).$$

The normal stresses σ_{xx} caused by bending across the beam are expressed by

$$\boxed{\sigma_{xx}(x,z) = \frac{M_y(x)}{I_y}z = -\frac{Q_z(\ell-x)}{I_y}z}.$$

The maximum normal stress is located at $(x = 0, z = \pm\frac{H}{2})$ and takes the value

$$|\sigma_{xx}|_{\max} = \frac{Q_z \, \ell}{I_y}\frac{H}{2}.$$

1.3 Closed Thin-Walled Sections

In closed section thin walled beams, the methodology is more or less identical compared to open sections. Also, the stress vector remains the same $\boldsymbol{\sigma} = \sigma_{xx}\mathbf{e}_x + \tau\mathbf{e}_s$. The difference lies in the general shape of the beam and subsequently the shape of the mid-line C, as there is not an 'edge' in the closed section. Thus, the curvilinear coordinate s is measured from a random point A in the cross section, which lies on the mid line C, meaning $s = 0$ at A (see figure 1.6). Similar to open sections, due to the exceptionally small nature of the cross section's thickness t, shear stress τ is assumed to be only a function of s, that is $\tau(s)$.

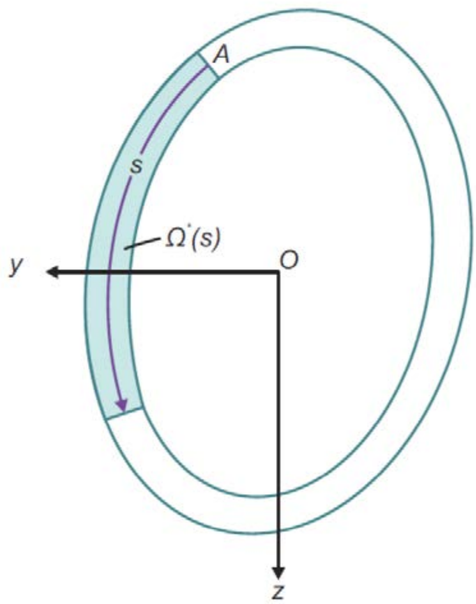

Figure 1.6: Single cell closed cross-section (adapted from [3]).

To calculate $\tau(s)$, two incisions are performed in the cross section, one is at A where $s = 0$ and the other at s. The area of the cross section between those two cuts is denoted as $\Omega^*(s)$, (see figure 1.6). The *shear flow* $q(s) = \tau(s)t(s)$ at s is calculated by

$$q(s) = \tau(s)t(s) = q_0 - \frac{1}{t(s)}\int_{\Omega^*(s)} \frac{\partial\sigma_{xx}}{\partial x} dA,$$

and q_0 is the shear flow at $s = 0$. Utilizing eq. 1.7 and substituting $\frac{\partial\sigma_{xx}}{\partial x}$, the above area integral yields

$$\boxed{q(s) = \tau(s)t(s) = q_0 - \left[\frac{Q_z}{I_y}S_y^*(s) + \frac{Q_y}{I_z}S_z^*(s)\right]}, \tag{1.18}$$

(I_y, I_z) are the principal moments of inertia of the cross section, and $(S_y^*(s), S_z^*(z))$ are area's $\Omega^*(s)$ static moments of inertia, about the central & principal y and z axes mentioned in the first subsection of this thesis.

Notes;

- All thickness related functions were not taken in consideration while calculating the area integral, due to the superficial changes of those functions in the thickness direction.

- Shear stress $\tau(s)$ has a positive sign when it runs counter-clockwise, the opposite is true when it runs clockwise.

- Equations (1.7) and (1.18) are very similar, with the only differentiating parameter being q_0, (shear flow at $s = 0$).

In order to calculate q_0, *shear flow theorem* is employed [4]:

$$\boxed{\oint_C \tau(s)ds = \frac{\nu}{1+\nu}\left(\frac{Q_z}{I_y}y_1^G - \frac{Q_y}{I_z}z_1^G\right)A_1}. \tag{1.19}$$

This theorem ensures that axial displacements u_x are univocal throughout the cross section. A_1 is surface's Ω_1 area and (y_1^G, z_1^G) are geometric center coordinates of Ω_1, in terms of a central & principal coordinate system. Equation (1.19) holds true if and only if, $\mathbf{Q}$ is applied at the cross section's shear center and is derived by [3] for $a_Q = 0$.

Substituting $\tau(s)$ to 1.19 from equation 1.18 yields:

$$q_0\beta - \frac{Q_z}{I_y}\oint_C \frac{S_y^*(s)}{t(s)}ds - \frac{Q_y}{I_z}\oint_C \frac{S_z^*(s)}{t(s)}ds = \frac{\nu}{1+\nu}\left(\frac{y_1^G}{I_y}Q_z - \frac{z_1^G}{I_z}Q_y\right)A_1,$$

where $\beta = \oint_C \frac{ds}{t(s)}$.

Shear flow q_0 is calculated by the previous equation,

$$\boxed{q_0 = \frac{Q_z}{\beta\, I_y}\left[\oint_C \frac{S_y^*(s)}{t(s)}ds + \frac{\nu}{1+\nu}y_1^G\,A_1\right] - \frac{Q_y}{\beta\, I_z}\left[\oint_C \frac{S_z^*(s)}{t(s)}ds + \frac{\nu}{1+\nu}z_1^G\,A_1\right]}. \tag{1.20}$$

Once q_0 is defined, the rest of the solution is calculated the same way as in open sections.

Total transverse load & torsional moment due to shear stresses distribution (1.18)

In closed section thin walled beams, it is proved that $F_y^\tau = Q_y$ and $F_z^\tau = Q_z$, which are the total forces in y and z directions respectively, are attributed to the shear stresses $\tau(s)$.That is the same case as in open sections, and the proof is the same as well, since the contribution of the term $q_0/t(s)$ is zero [2]:

$$\oint_C \frac{q_0}{t(s)} \underbrace{\cos\theta(s)}_{dz(s)/ds} t(s)ds = q_0 \oint_C dz(s) = 0 \quad \text{and} \quad \oint_C \frac{q_0}{t(s)} \underbrace{\sin\theta(s)}_{dy(s)/ds} ds = 0.$$

Regarding the torsional moment T^τ about the longitudinal x axis, which is caused by the shear stress distribution $\tau(s)$ featured in (1.18):

$$T^\tau \equiv \oint_C \tau(s) r_n(s) t(s) ds,$$

where $r_n(s)$ is the perpendicular distance between the tangent to the mid-line C and the cross section's geometric center O, see figure 1.3. Taking into consideration that $\oint_C r_n(s)\, ds = 2\, A_1$ and substituting $\tau(s)$ and q_0 from (1.18) & (1.20) respectively:

$$T^\tau = Q_z\, y_s - Q_y\, z_s,$$

where (y_s, z_s) are the shear center coordinates of the cross section and are completely dependent upon its geometric characteristics. These quantities are defined by the following two equations:

$$\boxed{y_s = \frac{1}{I_y} \left\{ \oint_C \left[\omega(s) z(s) t(s) + \frac{2\, A_1}{\beta} \frac{S_y^*(s)}{t(s)} \right] ds + \frac{\nu}{1+\nu} \frac{2\, A_1^2}{\beta} y_1^G \right\}}, \tag{1.21}$$

and

$$\boxed{y_s = \frac{1}{I_z} \left\{ \oint_C \left[\omega(s) y(s) t(s) + \frac{2\, A_1}{\beta} \frac{S_z^*(s)}{t(s)} \right] ds + \frac{\nu}{1+\nu} \frac{2\, A_1^2}{\beta} z_1^G \right\}}. \tag{1.22}$$

Shear center

In order for the shear stress distribution (1.18) $\tau(s)$ to be compliant with the applied loads (Q_y, Q_z), the following relation must hold true

$$T^\tau = T^Q \quad \forall\ (Q_y, Q_z), \tag{1.23}$$

[2]Integral $\oint_C dz$ turns to zero while **closed** curve C is integrated upon and ends up at the initial point.

where T^Q is the torsional moment caused by the transverse load (eq. (1.2))

$$T^Q = Q_z\, y_0 - Q_y\, z_0.$$

Finally, like in the open section case, in order for the $\tau(s)$, (1.18) relation to be true, coordinates (y_0, z_0) defining the transverse load $\mathbf{R}^\ell = Q_y\, \mathbf{e}_y + Q_z\, \mathbf{e}_z$ application point at $x = \ell$ beam end, must equal $y_0 = y_s$ and $z_0 = y_s$.

Note:

i. In many problems y-axis is a *symmetry* axis of the thin-walled cross section; in that case, the geometric center lies upon the symmetry axis ($z^G = z_1^G = z_s = 0$). Furthermore, if the z-axis is **not** central, equations (1.19) and (1.22) are altered as follows

$$\boxed{\oint_C \tau(s) ds = \frac{\nu}{1+\nu} \frac{Q_z}{I_y} (y_1^G - y^G) A_1}, \tag{1.24}$$

and

$$\boxed{y_s = \frac{1}{I_y} \left\{ \oint_C \left[\omega(s) z(s) t(s) + \frac{2\, A_1}{\beta} \frac{S_y^*(s)}{t(s)} \right] ds + \frac{\nu}{1+\nu} \frac{2\, A_1^2}{\beta} (y_1^G - y^G) \right\}}, \tag{1.25}$$

where y_1^G is the y coordinate of area's Ω_1 geometric center and y^G is the y -coordinate of the cross-section, with respect to a **non-central** coordinate system.

ii. Similarly to open sections, in case the transverse load $\mathbf{R}^\ell = Q_y \mathbf{e}_y + Q_z \mathbf{e}_z$ is applied to a point (ℓ, y_0, z_0) other than the shear center, a standard practice involves transferring $\mathbf{R}^\ell$ at the shear center of the cross section, while simultaneously considering the torsional moment $T = Q_z(y_0 - y_s) - Q_y(z_0 - z_s)$. In that case the main solution is comprised of two separate solutions;

   (a) Bending with a transverse load $\mathbf{R}^\ell$ placed at the cross section shear center & at the $x = \ell$ base of the beam.

   (b) Torsion with the torsional moment $T = Q_z(y_0 - y_s) - Q_y(z_0 - z_s)$.
   The shear stresses caused by T are described by the following formula;
   $\tau^T(n) = \frac{T}{2\, A_1 t}$, where $A_1 = \dfrac{1}{2} \oint_C r_n(s)\, ds$ is the area of the surface[3] enclosed by the mid-line C.
   Regarding the moment sign convention, the right hand rule applies.

[3]In simple geometries A_1 is easily computed as is, if not possible then $\oint_C \frac{\partial \Psi}{\partial n} ds = -2A_1$, where Ψ is the stress function [3].

1.3.1 Solution for A-Shell beam

Consider a tubular thin-walled beam, representing a rudimentary aerofoil. The cross section of the beam is reminiscent of an isosceles triangle, with vertex angle 2ψ. Its smallest side is part of a circle, with radius R, equal to the large sides, (see figure 1.7). The thickness of the beam is denoted as t (= constant), and it is significantly smaller than the mean radius R. Similarly to the C-channel cross section, the length of the A-shell is approximately $\ell = 10R$. The beam is loaded with a transverse force Q_z acting upon the $x = \ell$ beam end, Q_z is applied at a distance y_0 from the diameter, as illustrated in figure 1.7.

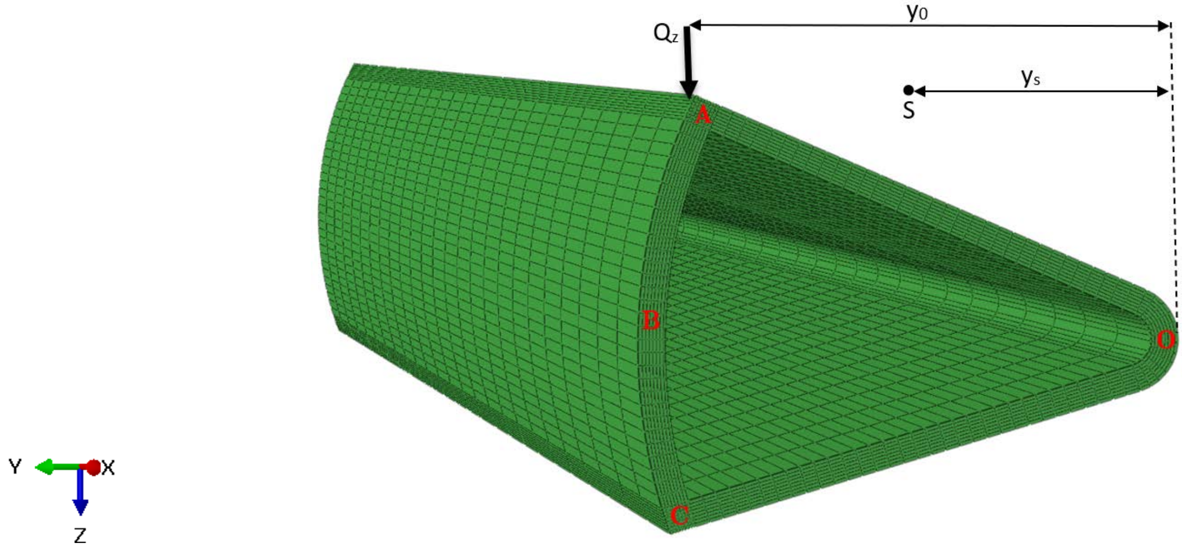

Figure 1.7: A-shell; Bending with transverse load of a closed thin-walled cross section.

Moving forward, the 'classic' way of calculating the shear center is used, where the shear stresses due to the transverse load are first calculated, then the torsion equation (1.14) is employed.

A non-central y-z coordinate system is used, alongside the respective polar coordinates (r, θ), (see figure 1.8). The y axis is a symmetry axis while the z axis is non-central.

First step involves calculating all geometric characteristics of the cross-section:

$$A_1 = R^2\,\psi, \quad L_C = 2\,R\,(1+\psi), \quad A = L_C\,t. \tag{1.26}$$

Referring to figure 1.8, alongside AO it is $y = y_{AO}(\psi) = R\cos\psi$ and $z = z_{AO}(s) = R\sin\psi$, whereas, alongside BO y and z may be expressed as $y = y_{CO}(s) = (R-s)\cos\psi$ and $z = z_{CO}(s) = (R-s)\sin\psi$, where s is the arc length alongside ABC. Thus, the quantities (I_y, y_G, y_1^G) are computed like so:

$$I_y = \int_\Omega z^2\,dA = \int_{BC\cup CO} z^2(t\,ds) = \left(\psi - \frac{\sin 2\psi}{2} + \frac{2}{3}\sin^2\psi\right)R^3\,t,$$

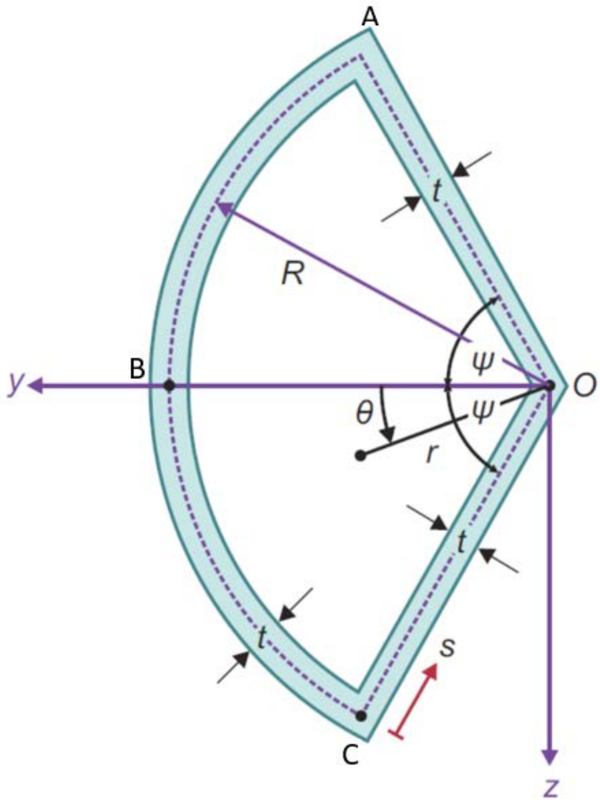

Figure 1.8: $y - z$ and (r, θ) coordinate systems. (adapted from [3]).

$$y_G = \frac{1}{A}\int_{\Omega} y\, dA = \frac{2}{A}\int_{BC\cup CO} y(t\, ds) = \frac{2}{2(1+\psi)R\,t}t\left\{\int_0^{\psi}(R\,\cos\theta)(R\,d\theta) + \int_0^{R}[(R-s)\cos\psi]\,ds\right\},$$

which leads to

$$y_G = \frac{\cos\psi + 2\sin\psi}{2(1+\psi)}R.$$

Similarly,

$$y_1^G = \frac{1}{A_1}\int_{\Omega_1} y\, dA = \frac{2}{R^2\,\psi}\int_{r=0}^{R}\int_{\theta=0}^{\psi}(r\,\cos\theta)(r\,dr\,d\theta),$$

where, Ω_1 is the area of the cross section enclosed by the mid-line C, and (r, θ) are the polar coordinates, (see figure 1.8). The last relation leads to

$$y_1^G = \frac{2}{3}\frac{\sin\psi}{\psi}R.$$

Shear stresses caused by the transverse force are computed by

$$\tau(s)^Q = \frac{q_0}{t(s)} - \frac{1}{t(s)}\frac{Q_z}{I_y}S_y^*(s), \quad S_y^*(s) = t\int_0^{s} z(s)ds, \tag{1.27}$$

where, q_0 is the shear flow [4]. Note that $\tau(s) > 0$ means that $\tau(s)$ runs counter-clockwise.

Following are the calculations of the static moment of inertia for the different sections of the profile, using equation (1.27).
Static moment of inertia at the curved ABC section of the profile is

$$S_y^{*(ABC)}(\theta) = t \int_{-\psi/2}^{\theta} (R\,\sin\theta'\,R\,d\theta') = R^2\,t(\cos\psi - \cos\theta),$$

where the angle θ is shown in figure 1.8. Moving to the AO and CO linear segments S_y^* is expressed by

$$S_y^{*(AO)} = t \int_0^{s_1} (R - s_1)\sin\psi\,ds_1 = t\,\sin\psi \left(s_1\,R - \frac{s_1^2}{2}\right)$$

and

$$S_y^{*(CO)} = t \int_0^{s_2} (s_2 - R)\sin\psi\,ds_2 = t\,\sin\psi \left(\frac{s_2^2}{2} - s_2\,R\right), \tag{1.28}$$

where $z_{AO} = (R - s_1)\sin\psi$ and $z_{CO} = (s_2 - R)\sin\psi$.

Thus, shear stress distribution is calculated by [5] (1.27):

$$\tau_{ABC}^Q(\theta) = \frac{q_0}{t} - \frac{Q_z}{I_y}R^2(\cos\psi - \cos\theta) \qquad (-\psi \le \theta \le \psi)\,, \tag{1.29}$$

$$\tau_{AO}^Q(s_1) = \frac{q_0}{t} - \frac{Q_z}{I_y}\sin\psi\left(s_1\,R - \frac{s_1^2}{2}\right) \qquad (0 \le s_1 \le R), \tag{1.30}$$

$$\tau_{CO}^Q(s_2) = \frac{q_0}{t} + \frac{Q_z}{I_y}\sin\psi\left(s_2\,R - \frac{s_2^2}{2}\right) \qquad (0 \le s_2 \le R). \tag{1.31}$$

The shear flow q_0 is calculated by the axial displacements uniqueness convention, (1.24):

$$\int_{-\psi}^{\psi} \tau_{ABC}^Q(\theta)(R\,d\theta) + \int_0^{s_1} \tau_{AO}^Q(s_1)ds_1 + \int_0^{s_2} \tau_{CO}^Q(s_2)ds_2 = \frac{\nu}{1+\nu}\frac{Q_z}{I_y}(y_1^G - y^G)A_1.$$

Next step involves substituting the values from $(\tau_{ABC}^Q(\theta), \tau_{AO}^Q(s_1), \tau_{CO}^Q(s_2), I_y, y_1^G, y^G, A_1)$ in the last equation, solving for q_0:

$$q_0 = \frac{Q_z}{R}D(\psi,\nu), \tag{1.32}$$

where

$$D(\psi,\nu) = \frac{A(\psi,\nu) + B(\psi,\nu)}{C(\psi,\nu)}, \tag{1.33}$$

[4] q_0 definition and convention have been established in 1.20

[5] The area moment of inertia I_y is left as is, purely for aesthetic and practical purposes.

$$A(\psi,\nu) = \nu\left[-3\,\psi(2\,\sin\psi + \cos\psi) + 4(1+\psi)\sin\psi\right], \tag{1.34}$$

$$B(\psi,\nu) = 12(1+\nu)(1+\psi)(\psi\cos\psi - \sin\psi), \tag{1.35}$$

$$C(\psi,\nu) = 2(1+\nu)(1+\psi)^2\left[6\,\psi + 4\sin^2\psi - 3\,\sin 2\psi\right]. \tag{1.36}$$

Torsional moment T^τ about the non-central x axis caused by the shear stress distribution τ^Q is [6]

$$T^\tau = \int_{-\psi}^{\psi} \tau^Q_{ABC}(\theta)\,R\,\underbrace{[t(R\,d\theta)]}_{dA} = \ldots = 2\,q_0\,R^2\,\psi + 2\,Q_z\,R\,F(\psi,\nu),$$

where

$$F(\psi,\nu) = \frac{-\psi\cos\psi + \sin\psi}{\psi - \frac{1}{2}\sin 2\psi + \frac{2}{3}\sin^2\psi}, \tag{1.37}$$

and relation (1.29) was used for the calculation of the integral above. Substituting q_0 in the last relation leads to the following expression for the torsional moment T^τ:

$$T^\tau = Q_z\,R\left[\psi\,D(\psi,\nu) + 2\,F(\psi,\nu)\right].$$

In case the transverse force is placed at the shear center S, the torsional moment T^Q is $T^Q = Q_z\,y_s$, y_s is the y-coordinate of the cross section's shear center. Thus, the condition $T^\tau = T^Q$ leads to

$$y_s = R\left[\psi\,D(\psi,\nu) + 2\,F(\psi,\nu)\right],$$

where $D(\psi,\nu)$ and $F(\psi,\nu)$ are defined in (1.33) and (1.37).

Note:

- In curtain applications the vertex angle ψ may vary from $0°$ up to $90°$. If the angles are very small (less than $5°$) the shear center location lies outside of the cross section (in front of the curved ABC section).

In case the transverse load is applied at a point other than the shear center ($y_0 \neq y_s$), then there are additional shear stresses τ^T caused by the torsion of the beam. To calculate these additional shear stresses Q_z is "transferred" at the shear center, and the torsional moment $T = -(y_s - y_0)Q_z$ is considered. To calculate these shear stresses τ^T the first Bredt equation is used [3]

$$\tau^T = \frac{T}{2\,A_1\,t} = -\frac{(y_s - y_0)Q_z}{2\,R^2\,\psi\,t} = \text{const.}^{7}$$

[6] shear stresses at branches AO and CO do not contribute to the torsional moment equation about the x axis.

[7] τ^T is constant all across the thickness of the beam unlike in open sections.

The total shear stress in the cross section is

$$\tau(s) = \tau^Q(s) + \tau^T,$$

where $\tau^Q(s)$ is defined in (1.29), (1.30), and (1.31).

Note:

- In case $y_0 \leq y_s$ the maximum shear stress appears at points A and C of the two linear sections, respectively.

$$|\tau|_{\max} = |\tau^Q_{AO}|_{\max} + \tau^T \equiv |\tau^Q_{CO}|_{\max} + \tau^T,$$

- In case $y_s \leq y_0$ the maximum shear stress appears at the middle point B of the curved ABC section.

$$|\tau|_{\max} = |\tau^Q_{ABC}|_{\max} + \tau^T.$$

Similarly to the C-shell (open cross section), the bending moment distribution along the beam's length is

$$M(x) = -Q_z(\ell - x)$$

and the normal stress distribution σ_{xx} across the beam is determined by

$$\sigma_{xx}(x,z) = \frac{M_y(x)}{I_y} z = -\frac{Q_z(\ell - x)z}{\left(\psi - \frac{1}{2}\sin 2\psi + \frac{2}{3}\sin^2\psi\right) R^3\, t}.$$

The maximum absolute value of the normal stress appears at $(x = 0, z = \pm R\sin\psi)$, and takes the following value

$$|\sigma_{xx}|_{\max} = f(\psi)\frac{Q_z}{R^2\, t}, \qquad f(\psi) = \frac{\sin\psi}{\psi - \frac{1}{2}\sin 2\psi + \frac{2}{3}\sin^2\psi}.$$

Chapter 2

Finite Element Analysis

This is the final chapter of the present thesis and comprises of two main sections. The first section is a presentation of all the steps necessary to create both numerical thin-walled beam models. Generating both the A-shell and C-channel models for this analysis involved the utilization of the 'input file' method found in ABAQUS/Standard [1], (commercial software) and the use of Microsoft Excel. At the end of this chapter, section 2.4 can be found, which is devoted to comparing the numerical solution derived from ABAQUS to the analytical solution, which was presented in chapter 1 (sections 1.2.1 and 1.3.1). In that section, the results for both the normal (σ_{xx}) and shear stresses ($\tau, \sigma_{xy}, \sigma_{xz}$) of the numerical solutions are compared to the corresponding analytical solutions. The main purpose of this thesis is this comparison.

2.1 Cross Section Design In ABAQUS/CAE

The make-up procedure for both beams is identical. The process can be divided into two major steps.

The first step is concerned with designing the two-dimensional profile of the beam, i.e., the cross-section of the beam. Utilizing the CAD capabilities of ABAQUS/CAE, the profile can be designed with relative ease. Once that is done, a process called partitioning may take place. Partitioning of the two-dimensional profile involves parting the geometric shape into smaller, simpler shapes. This method ensures that the spatial discretization (mesh generation) of the model is done properly, in a more efficient and systematic manner. Having partitioned the 2D profile, nodes must be created, using what is referred to in ABAQUS as 'seeds'. Thus, after the insertion of seeds/nodes in each partitioned area, the part (cross section) can be meshed. The element type used in the 2D profile is 'CPS4R', which are 4-node bilinear plane stress quadrilateral elements. Finally, to acquire a primitive form of the input file, a false job [1] should be performed. (In ABAQUS, a simulation of any kind is referred to as a job.) This procedure concludes the first step.

[1]False job implies that neither boundary conditions nor material properties are applied to the model.

2.1.1 Mesh Generation Using Microsoft Excel

Second step in line, is the formation of the three-dimensional shell. In order to export the geometry dimensionally, nodes and elements are acquired from the primitive input file (previous step). These nodes and elements refer to two dimensions, meaning that there are only two specific coordinates per node and only four specific nodes per element. In the present thesis, Microsoft Excel was utilized in order to modify nodes and elements into their 3D counterparts; an explanation of this process follows.

After inserting the 2D nodes and elements into an Excel sheet, the modification process may commence. The method used in this thesis requires three separate sets of nodes to be created; these node sets will also be of great value later on for the boundary condition application. The first set corresponds to the $x = 0$ base of the beam; thus, a third coordinate with a value of zero is added to every node of the 2D model. This modification converts 2D nodes into the 3D nodes of the $x = 0$ base of the beam.

The second set is the immediate layer of nodes after the $x = 0$ base layer; the axial distance between those two sets of nodes is chosen arbitrarily by the user. That distance controls how dense the mesh is going to be in the axial direction, meaning how many layers of nodes it will take to form the entire length of the beam, all the way through its $x = \ell$ base. In essence, if the user so desires, theoretically the beam could be comprised of only two layers of nodes, with an axial node-to-node distance equal to the length of the beam, ℓ. In practice though, that model would be insufficient, since there would be no intermediate nodes and elements to accurately describe the strains and stresses curves in that area. So, a node-to-node distance of one tenth to one fifteenth the length of the beam seems to be adequate. Thus, each node of this set is assigned a third coordinate equal to the quantity described above.

Additionally, a number is added to every node label, that number is arbitrarily chosen, since its selection does not affect the model. In spite of that, the number of choice is advised to be at least an order of magnitude larger than the greatest node label, so there is a way to differentiate between node layers. These two node sets form the first layer of elements.

The third and final set of nodes that must be created using Excel corresponds to the $x = \ell$ base of the beam. Every node of that set gets a third coordinate equal to the length of the beam. In a similar fashion with the second node set, a number is added to each node label of that set. That number usually is equivalent to the number added in the labels of the second set, multiplied by the number:[(total node layers) -1].

Soon after converting the 2D nodes into 3D, elements must be converted as well. Each 2D element consists of 4 nodes; the conversion requires 4 extra nodes to be added to each and every element. The nodes to be added are equal to the initial nodes of the 2D element plus the arbitrary number mentioned above (e.g. 10000). The 8-node elements that are produced correspond to the $x = 0$ base of the beam (first layer of elements). This is the only elemental layer that has to be created manually. The 8-node element type will be assigned in the new 3D input file.

Node label example:

The nodes with labels 1800, 11800, and 501800 correspond to the opposing nodes of the first ($x = 0$ base), second, and final ($x = \ell$ base) node layers respectively (arbitrary number = 10 000). In this example, there are 51 node layers. The node label numbering is up to the user and could be different. The node label and the node-to-node distance should not be confused; the node label represents a node's name, whereas the node-to-node distance refers to the axial node coordinate, x. That way of systematic node numbering will be quite convenient in later stages of the analysis, where nodes and elements are needed for boundary condition application and stress-strain paths across the beam.

2.1.2 Input File Assembly

Finally, to export the 2D profile in the third dimension, an input file with the 3D quantities created in Excel, paired with all necessary ABAQUS commands must be formulated. To make the new 3D input file easier to read and more manageable, two separate txt input style files are created containing the 3D nodes and 3D elements respectively. These files are inserted in the new input file via the ABAQUS command [2] *INCLUDE, and the parameter 'INPUT=' is set equal to the name of the 3D node/element file, respectively. Although the 2D nodes and elements have been converted to 3D, there are still some ABAQUS commands necessary to export the geometry into the third direction.

Regarding the node file, the aforementioned 3 3D node sets are created using the command *NODE, paired with the parameter 'NSET=' set to the desired node set name (user specified). A necessary command to fill in with nodes the entire 3D section of the beam is *NGEN. Nodes get filled in between the second and $x = \ell$ layers of nodes respectively, with an increment equal to the previously mentioned arbitrary number (e.g., 10 000).

Similarly, for the element file the command *ELSET alongside with the parameters 'TYPE=' and 'ELSET=' are used. In this analysis, the element type used is 'C3D8H', these are isoparametric, tetrahedral, 8-node continuum elements. The 'ELSET=' is set to LAYER_1 (user specified). Next, the command employed to create all the elements of the model is *ELCOPY, paired with all necessary parameters. This command and parameters are repeated as many times as needed to create all the element layers.

This procedure concludes the mesh generation and the consequent creation of the 3D shell.

2.2 Material Properties

In this section of the 3D input file, a material is assigned to the beam. Initially, an additional txt input style file is created. In this new file, *ELSET command is used with the parameter ELSET=' set to ALL_EL (user specified). The data lines that follow contain all the element layers that have been previously generated. This command accumulates all the elements of

[2] All ABAQUS commands and parameters mentioned in this thesis (e.g. *INCLUDE, INPUT=) have been sourced from [2].

the beam in one set. Said element set will be assigned the material properties. The insertion of this data file in the main 3D input file follows. The assignment process commences with the command *SOLID SECTION and the parameter 'ELSET=' set to ALL_EL. Next, the commands *MATERIAL and *ELASTIC follow one after the other. The *ELASTIC command implies that the material used is of elastic nature. The material in this thesis is assumed to be linear elastic; thus, the data line input is the Young's modulus E and Poisson's ratio ν.

2.3 Boundary conditions

Boundary condition application is a necessary step before conducting the numerical analysis. BCs are applied upon the mesh generated; computational mesh generation was thoroughly examined in the previous section. In this analysis, two types of **kinematic** boundary conditions are used. Both kinematic BCs are applied at the $x = 0$ end of the beam; the differences and the concept behind each BC are explained in the following subsections.

2.3.0.1 Kinematic BC

Two types of kinematic boundary conditions were employed; all kinematic BCs are initiated using the *BOUNDARY command.

1. The first BC includes two arguments; first is the node set at $x = 0$ base of the beam, and the second one is ENCASTRE. Argument ENCASTRE, sets all degrees of freedom of every node in this set to zero. The degrees of freedom of each node in the present analysis are the displacement components (u_x, u_y, u_z).

2. The second BC, let's call it 'the 3-point pinning method', includes only three nodes of the $x = 0$ beam base. These nodes are usually spread throughout that surface, for example two nodes at the far end corners of the beam and one node at the axis origin. This BC allows the beam to move in space more freely, since it is not restricted in every base node (unlike ENCASTRE argument). Three nodes are the minimum necessary points of contact to ensure no rigid body translations or rotations occur at $x = 0$ beam end.

A Shell Kinematic BC

The A shell is given the ENCASTRE BC, since it makes little to no difference if the three-point pinning method is used.

C shell Kinematic BC

During the numerical analysis, it was observed that the ENCASTRE method restricted the inherent warping tendencies of the C-shell, decreasing significantly the shear stresses all across the beam. Consequently, analytical and numerical solutions did not coincide.

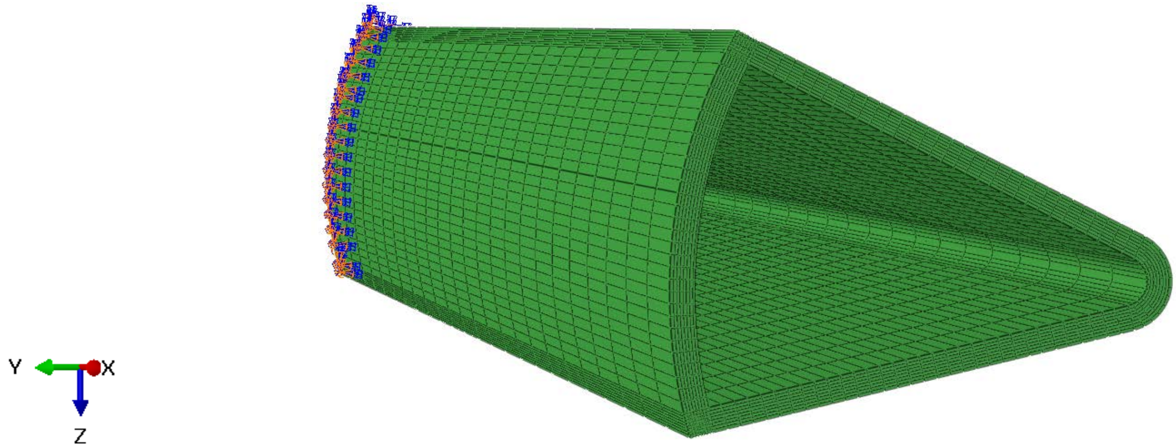

Figure 2.1: A-shell; ENCASTRE boundary condition at $x = 0$ beam end.

Thus, the 3-point pinning method was employed. The C-channel beam is an open section, so it deforms to a much greater extent compared to a similar closed section. Stresses are proportional to strains. So a restrictive boundary condition at the $x = 0$ base like ENCASTRE decreases the torsional behavior of the cross section, subsequently decreasing the shear stresses. At the same time, the normal stresses are increasing. These normal stresses originate from the restricted $x = 0$ base and counter the beam's warping tendencies.

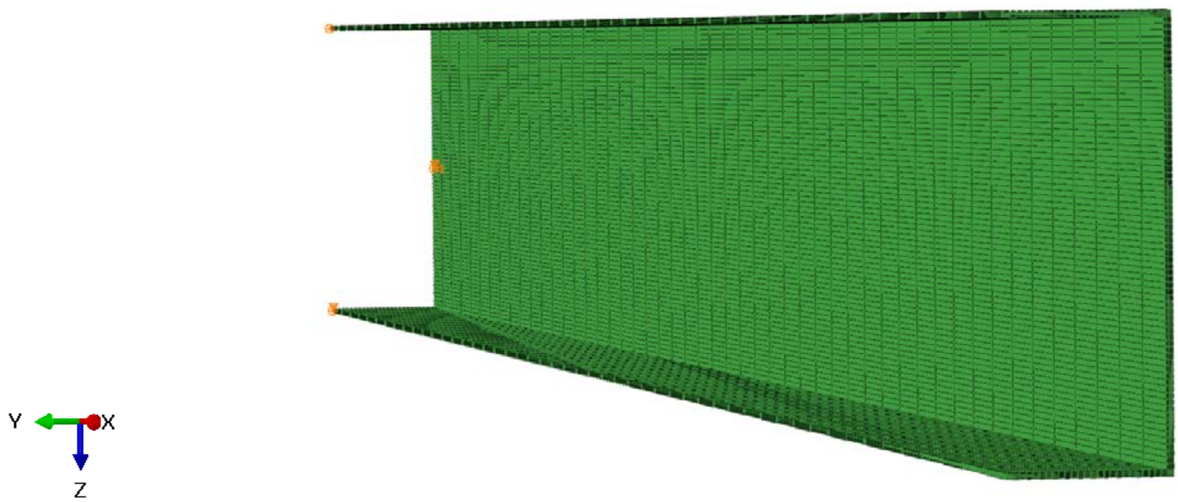

Figure 2.2: C-shell; '3-point pinning method' boundary condition at $x = 0$ beam end.

2.3.0.2 Transverse load BC

To place a static load BC at the $x = \ell$ base of the beam, the commands *STEP and *STATIC must be used. The *STEP command initiates a 'loading step', and *STATIC implies that the load is applied in a single time increment. This can happen due to the fact that the present analysis is linear and elastic, with minute displacements and strains. So, the convergence of the solution is not affected by the instant application of the concentrated load. The concentrated load itself is placed using the command *CLOAD, and a data line that defines the node of load application, orientation, and magnitude. In the case of the C-shell beam, the load is applied at the central node of the web, with coordinates $(y_0, z_0) = (0, 0)$ (see Fig. 2.3a). Regarding the A-shell, the load is applied at the central node of the semi-circular side of the beam, with coordinates $(y_0, z_0) = (38.1, 0)$, all length units are measured in millimeters (see Fig. 2.3b).

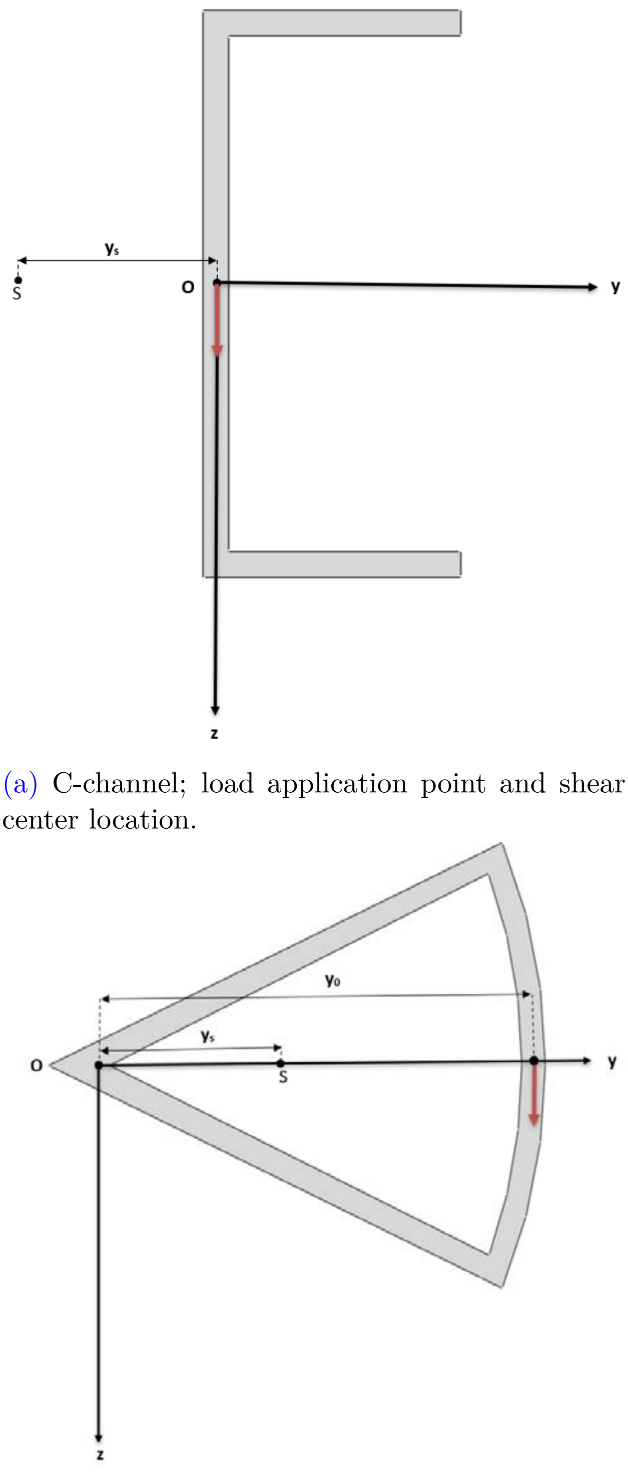

(a) C-channel; load application point and shear center location.

(b) A-shell; load application point and shear center location.

Figure 2.3: Load application points and shear center locations for C-channel (subfigure (a)) and A-shell (subfigure (b)) thin-walled beams.

2.4 Result Normalization

This section contains a systematic method for normalizing both numerical and analytical results. This step is performed so the results appear more uniform, making it easier to reach conclusions.

All stresses are normalized with the greatest normal stress $\sigma_{xx}^{\max}(x, h/2)$ found in each beam, and all lengths are normalized with the contextual dimensions shown below.

$$\bar{\ell} = x/\ell, \quad \bar{s}_1 = \left(\frac{s_1}{H}\right)_{\mathrm{C}} = \left(\frac{s_1}{\psi\, R}\right)_{\mathrm{A}}, \quad \bar{s}_2 = \left(\frac{s_2}{h}\right)_{\mathrm{C}} = \left(\frac{s_2}{R}\right)_{\mathrm{A}}, \quad \bar{s}_3 = \left(\frac{s_3}{h}\right)_{\mathrm{C}} = \left(\frac{s_3}{R}\right)_{\mathrm{A}},$$

$$\bar{\tau} = \frac{\tau}{\sigma_{xx}^{\max}\left(x, \frac{H}{2}\right)}, \qquad \bar{\sigma}_{xx} = \frac{\sigma_{xx}}{\sigma_{xx}^{\max}\left(x, \frac{H}{2}\right)}.$$

Where the indexes C and A declare the cross section. Quantities that do not have an index

are universal for both beams. The bar over the symbols is used to denote that the 'bared' quantity has been normalized.

2.5 Numerical Results

2.5.1 Model Description

In the previous sections, it became apparent that for both beam models, the makeup process is almost identical. Due to the inherent differences of each beam, some parameters and dimensions are dissimilar. In this section, all beam dimensions and parameters are presented along with the numerical results for each beam model.

C shell

The C shell is a normal C-channel prismatic beam. The height of the wed is denoted as H, whereas the length of the flanges is denoted as h. The shell thickness is t. The beam consists of 50 elemental layers, with each layer containing 1 216 elements, for a total of 60 800 elements.

A shell

The A shell beam represents a rudimentary aerofoil. The profile of the beam is reminiscent of an isosceles triangle, with a vertex angle $2\,\psi$. Its smallest side is part of a circle, with radius R, equal to the two large sides. Also, the tail of the beam has been given a fillet, aimed at concentrated stress reduction. The fillet radii are t and $2\,t$, for the internal and external areas of the closed shell respectively, where t represents the shell thickness. Regarding the mesh used, the beam consists of 25 elemental layers, each layer contains 976 elements, for a total of 24 400 elements.

The tables that follow contain all dimensional and loading parameters for both beams, as well as the material mechanical properties. All coordinates refer to the coordinate systems shown in Fig. 2.3. In the C shell, the system is neither central nor principal. In the A shell, the system is central but not principal. In the tables, y_s denotes the y-coordinate of the shear center and (y_0, z_0) are the coordinates of the point of application of the transverse load.

C shell	H	h	ℓ	t	y_s	z_s	y_0	z_0	I_y	J	Load
Value	140	51.5	1 500	2	-18	0	0	0	1.467×10^6	648	20
Units	mm	mm	mm	mm	mm	mm	mm	mm	mm^4	mm^4	N

Table 2.1: C-channel beam; geometric and loading parameters.

A shell	R	ψ	ℓ	t	y_s	z_s	y_0	z_0	I_y	Load
Value	42	20	500	2	25	0	38.1	0	1.55×10^4	20
Units	mm	degrees	mm	mm	mm	mm	mm	mm	mm^4	N

Table 2.2: A-shell beam; geometric and loading parameters.

Construction steel	σ_o	E	ν
Value	250	200	0.3
Units	MPa	GPa	–

Table 2.3: Material properties.

In thin-walled beam theory, it is stated that the thickness of the beam, t, must be significantly smaller than the rest beam dimensions. Additionally, according to Saint-Venant's beam theory, the length of the beam should be quite larger than the rest dimensions. These two constraints lead to the selection of $t = 2$ mm and $\ell_A = 500$ mm and $\ell_C = 1\,500$ mm for both beams respectively. Lastly, this analysis is performed within the linear-elastic boundaries of the material. Thus, a concentrated load of 20 N was selected in both cases. Consequently, the resultant stresses are way below the yield stress, and remain in the linear-elastic region.

2.5.2 Normal Stress σ_{xx}

According to the analytical solution, the normal stress in the beam is described by the following formula:

$$\sigma_{xx} = -\frac{Q_z(\ell - x)}{I_y} z. \tag{2.1}$$

Formula (2.1) describes the normal stress distribution in both A and C shell beams, and states that σ_{xx} is a linear equation of x and z. The numerical solutions confirm that with some minor deviations (Figs 2.4 & 2.5), almost exclusively near the $x = 0$ beam end. According to Saint-Venant's beam theory, all boundary conditions at the beam end $x = 0$ are replaced with loads and moments. Thus, it is normal for the solution to be affected near that boundary. In this case, the $x = 0$ base of the beam is affected where the kinematic BCs are applied.

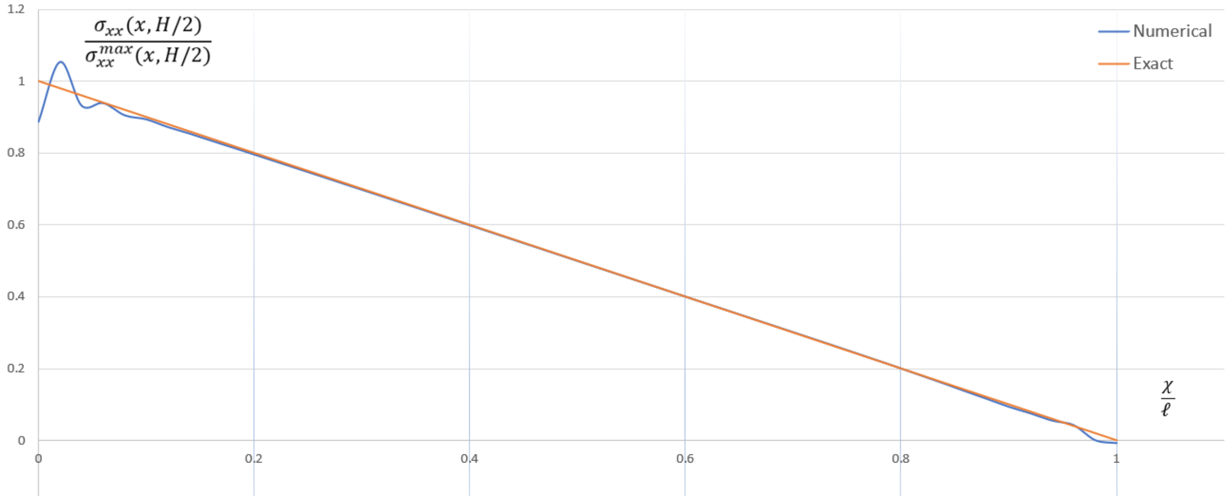

Figure 2.4: C-channel; distribution of $\sigma_{xx}(x, H/2)$ in the longitudinal x-direction. The numerical solution is compared to the exact.

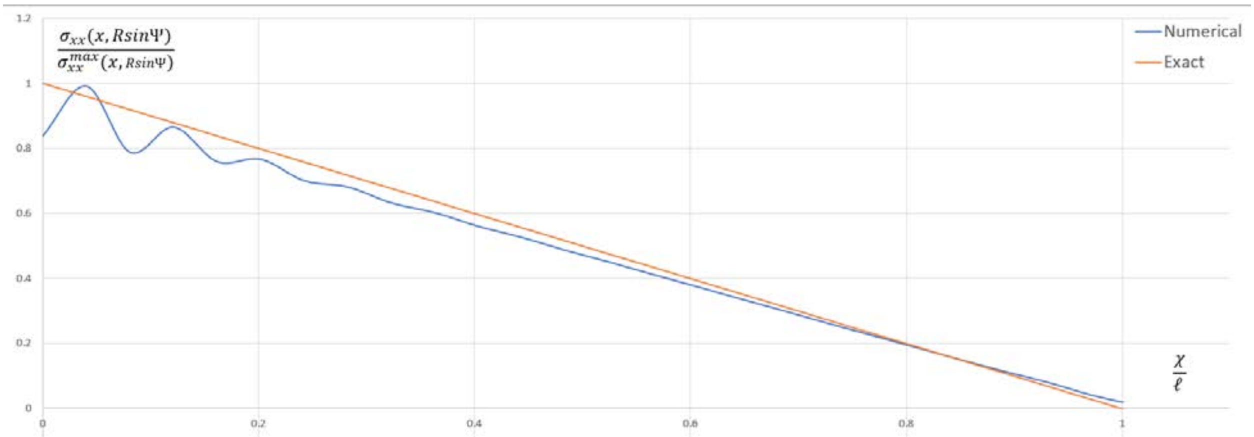

Figure 2.5: A-shell; distribution of $\sigma_{xx}(x, R\sin\psi)$ in the longitudinal x-direction. The numerical solution is compared to the exact.

2.5.3 Curvilinear Stresses τ_{xs}, τ_{xy}, and τ_{xz}

The analysis performed in ABAQUS involved the use of a non-central coordinate system $y-z$, where the y axis is the cross-section symmetry axis. According to the thin-walled beam theory, the non-zero components of the stress tensor are $(\sigma_{xx}, \sigma_{xs}, \sigma_{xn})$ or $(\sigma_{xx}, \sigma_{xy}, \sigma_{xz})$, in the curvilinear or Cartesian coordinate system respectively. In the previous chapter (1.1.2), it was concluded that $\sigma_{xn} \cong 0$, consequently, the only surviving shear stress component is $\sigma_{xs} \equiv \tau$. Shear stress τ runs along the beam's mid-line C, making it parallel to its cliff face.

In Abaqus, only the aforementioned Cartesian coordinate system (x, y, z) is used. In geometries where the mid-line C is not parallel to the x or y axis respectively, the curvilinear shear stress $\tau \equiv \sigma_{xs}$ cannot be directly extracted since, $\tau \neq \sigma_{xy}$ and $\tau \neq \sigma_{xz}$. Thus, τ is acquired from

$$\tau = \sqrt{\sigma_{xy}^2 + \sigma_{xz}^2}\,. \tag{2.2}$$

Considering the C shell, where the beam's mid-line C is constantly parallel to either z (web) or y axis (flanges), only σ_{xz} or σ_{xy} component survives the stress transform (2.2), for the web and flanges, respectively. Whereas, in the case of the A shell, neither the large sides nor the small semi-circle side are parallel to y or z axes, so the employment of the relation (2.2) is necessary.

In the upcoming pages, a series of graphs follow. These graphs compare the numerical solutions derived with the help of Abaqus to the analytical solutions presented in chapters 1.2.1 and 1.3.1, for both the C shell and A shell thin-walled beams, respectively.

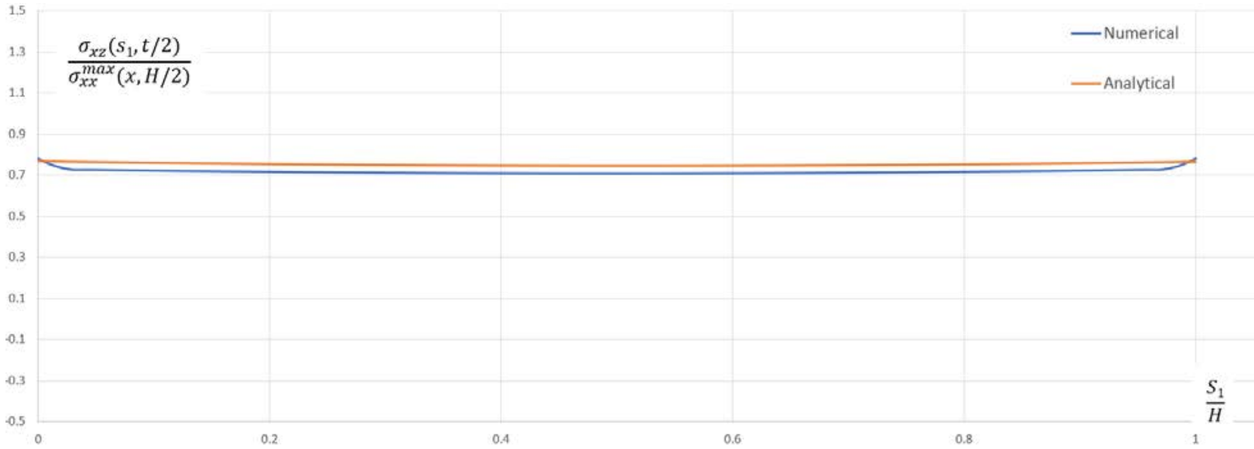

Figure 2.6: C-channel; normalized distribution of $\tau \equiv \sigma_{xz}(s_1, t/2)$ across the height of the web H. The numerical solution is compared to the analytical.

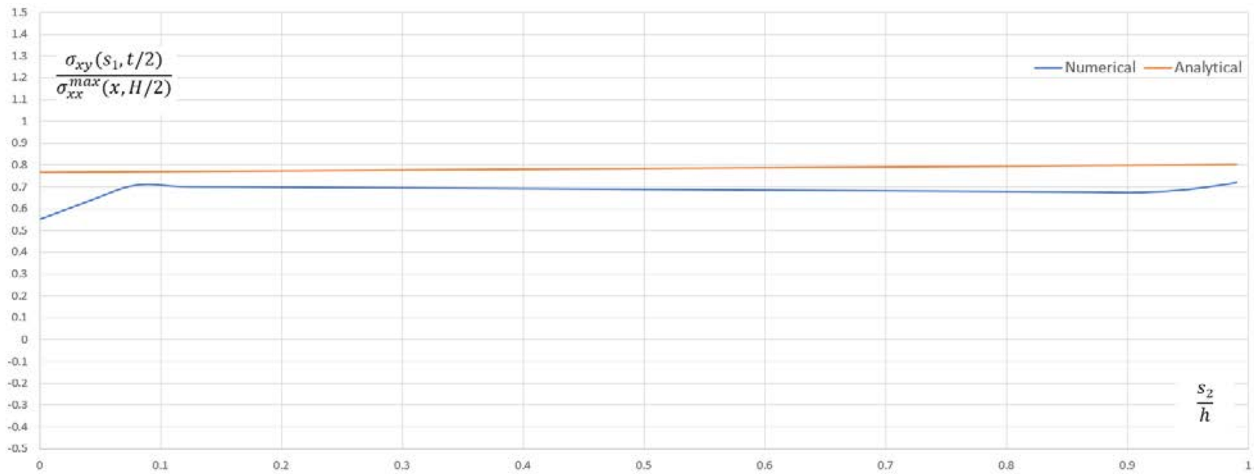

Figure 2.7: C-channel; normalized distribution of $\tau \equiv \sigma_{xy}(s_2, t/2)$ across the length of the top flange h. The numerical solution is compared to the analytical.

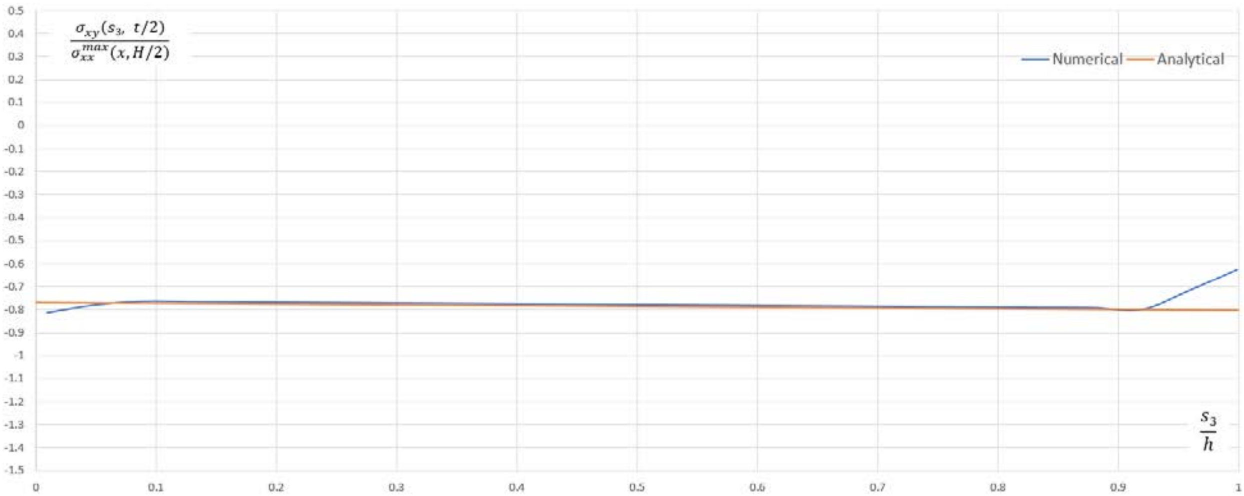

Figure 2.8: C-channel; normalized distribution of $\tau \equiv \sigma_{xz}(s_3, t/2)$ across the length of the bottom flange h. The numerical solution is compared to the analytical.

As illustrated in figures (2.6), (2.7), and (2.8), the numerical solution for the C channel section appears to approximate the exact solution quite accurately, with an error of about 7%.

Following these series of graphs, down below the equivalent graphs for the A-shell cross section are presented.

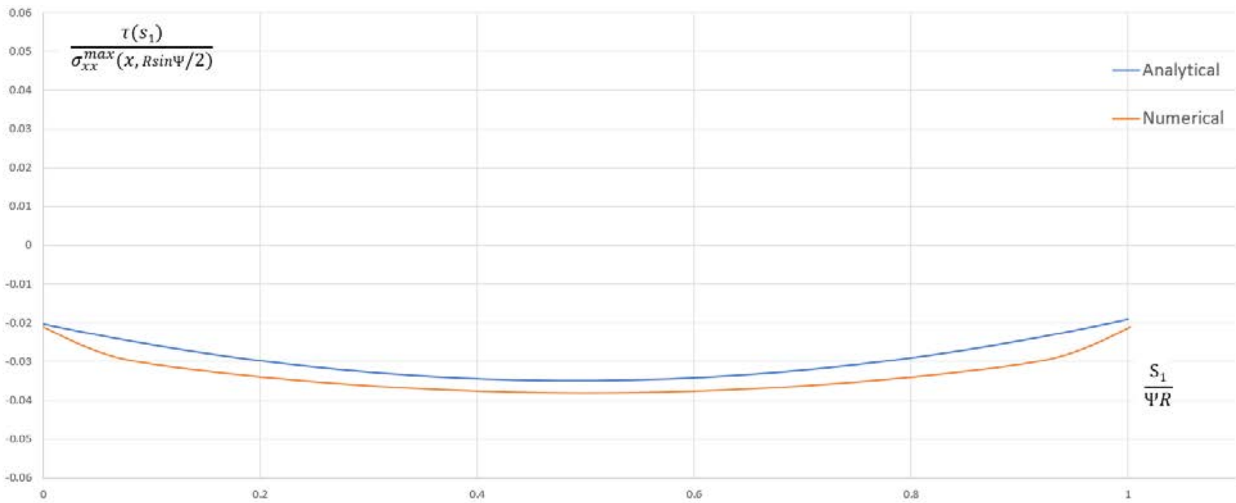

Figure 2.9: A-shell; normalized distribution of $\tau \equiv \tau(s_1)$ across the length of the curved section ABC of the aerofoil. The numerical solution is compared to the analytical.

Figure 2.10: A-shell; normalized distribution of $\tau \equiv \tau(s_2)$ across the length of the upper side AO of the aerofoil. The numerical solution is compared to the analytical.

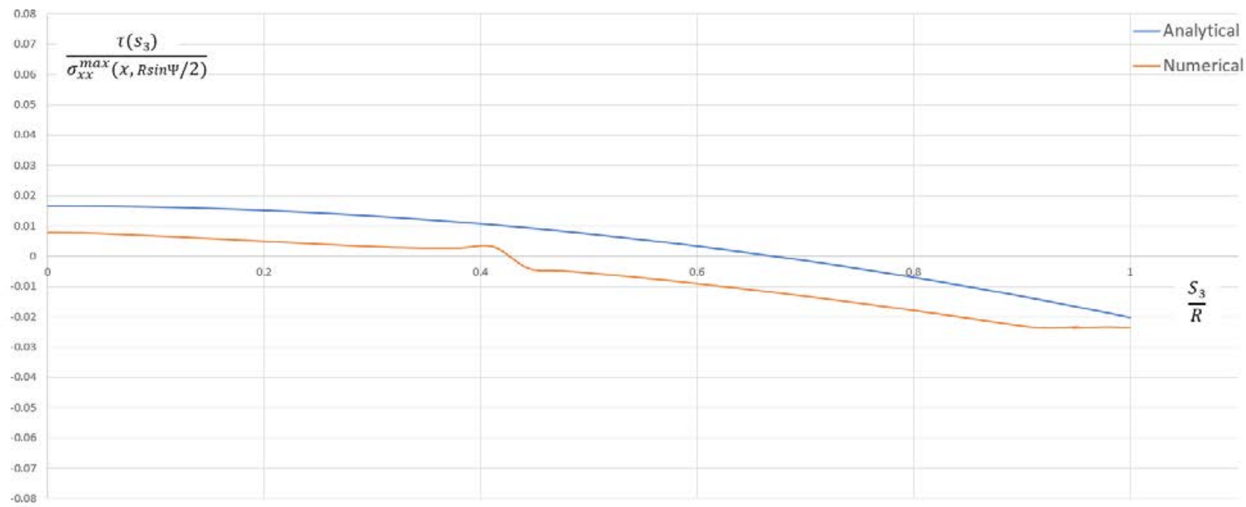

Figure 2.11: A-shell; normalized distribution of $\tau \equiv \tau(s_3)$ across the length of the lower side CO of the aerofoil. The numerical solution is compared to the analytical.

In the case of the A-shell, the numerical approximation is quite accurate as well, with the error being around 7% in most areas. Only in the upper and lower sides AO and CO respectively, of the aerofoil is there a significant deviation from the analytical solution observed; however, the magnitude of the shear stresses is way smaller in that area (close to zero). Additionally, the numerical solution curve 'follows' the analytical one with both curvatures being almost identical. Thus, this deviation is considered of minute importance.

It is also worth mentioning that the numerical solution remains accurate in an area of the beam away from both $x = 0$ and $x = \ell$ beam ends where the Saint-Venant's boundary conditions are applied. This area of numerical accuracy lies within the $\ell/5 \leq x \leq 4\ell/5$ vicinity.

2.5.4 Shear Center; Analytical and Numerical Solutions

This section contains a comparison between the Analytical and the Numerical solution, in case the transverse load is applied to the shear center of the thin-walled beam (either the A-shell or the C-shell).

The shear stress τ is the sum of two functions, as it was concluded in sections 1.2.1 and 1.3.1. Even though the concept of the solution is the same for both the open and the closed types of cross sections, the behavior each beam exhibits under load is unique. The main reason for this difference in behavior is attributed to the cross section geometry and the shear flow. In open cross section beams, the shear flow q is zero. The shear stress τ varies linearly across the thickness and changes sign. In closed cross section beams on the other hand, the shear flow q is not zero, and the shear stress τ remains constant in the thickness direction.

As a result, open sections are way more sensitive to load placement and the shear stress's τ major component is the additional shear stress τ^T (1.2.1) caused by torsion. In case the transverse load is placed in the shear center of an open cross section, the shear stress magnitude $|\tau|$ diminishes across the beam.

In contrast, closed cross sections are not as sensitive to load placement and thus, in case the transverse load is placed in the shear center of the cross section, the shear stress magnitude $|\tau|$ drops by a much smaller margin compared to open sections.

2.5.4.1 Abaqus Modeling of Shear Center

In the case of the C-channel, the shear center lies outside of the cross-section. As a result, there is not a physical node where the load may be applied. In such circumstances, a method of generating a separate **auxiliary node** that is later on 'tied' to the original nodes of the $x = \ell$ base of the beam is employed; an explanation of this method follows.

This process begins with the 3D beam in the Abaqus CAE environment. The first step involves the creation of a *reference point* via the drop-down menu box denoted as 'Tools'. After the reference point is created, a constraint must be set; from the drop-down model tree, the option 'constraint' is chosen followed by 'Rigid body' (then continue). A selection box appears (Edit Constraint) the 'Tie (nodes)' option is selected followed by the large arrow in the top right corner of that selection box. The 'Sets...' option is then selected, found in the bottom right corner of the viewport; a selection box (region selection) appears, the node set that corresponds to the nodes of the $x = \ell$ base of the beam is selected (then continue). The 'Tie (nodes)' option is already selected in the selection box (Edit Constraint), so the reference point arrow is selected (bottom of the current selection box). Lastly, the reference point is selected manually with the cursor by the user (viewport). This process concludes the creation of the auxiliary node. The load can now be placed on that node and the analysis may commence.

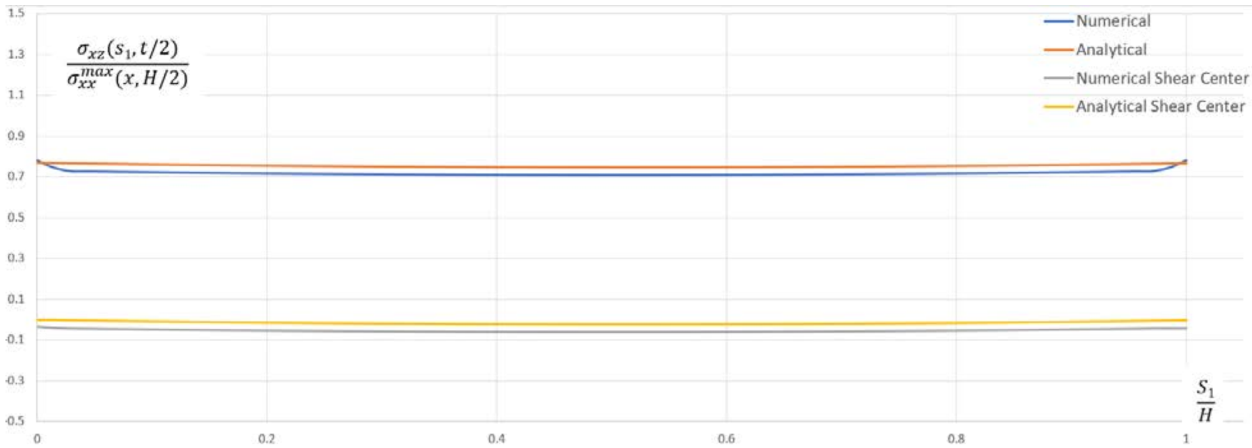

Figure 2.12: C-shell; normalized distribution of $\tau \equiv \sigma_{xz}(s_1, t/2)$ across the height of the Web H. The numerical solution is compared to the analytical, the transverse load is applied at the *shear center*.

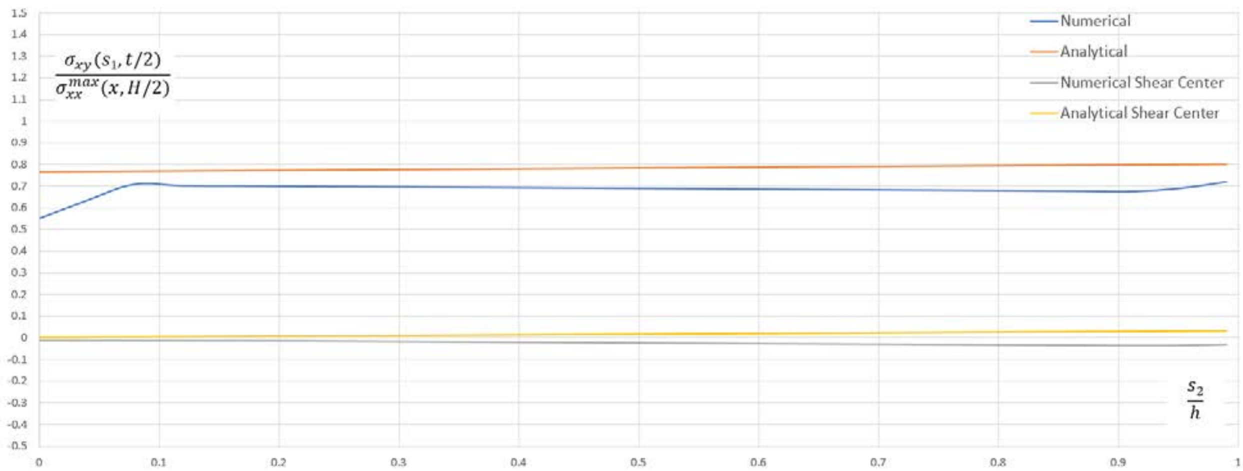

Figure 2.13: C-shell; normalized distribution of $\tau \equiv \sigma_{xy}(s_2, t/2)$ across the length of the top flange h. The numerical solution is compared to the analytical, the transverse load is applied at the *shear center*.

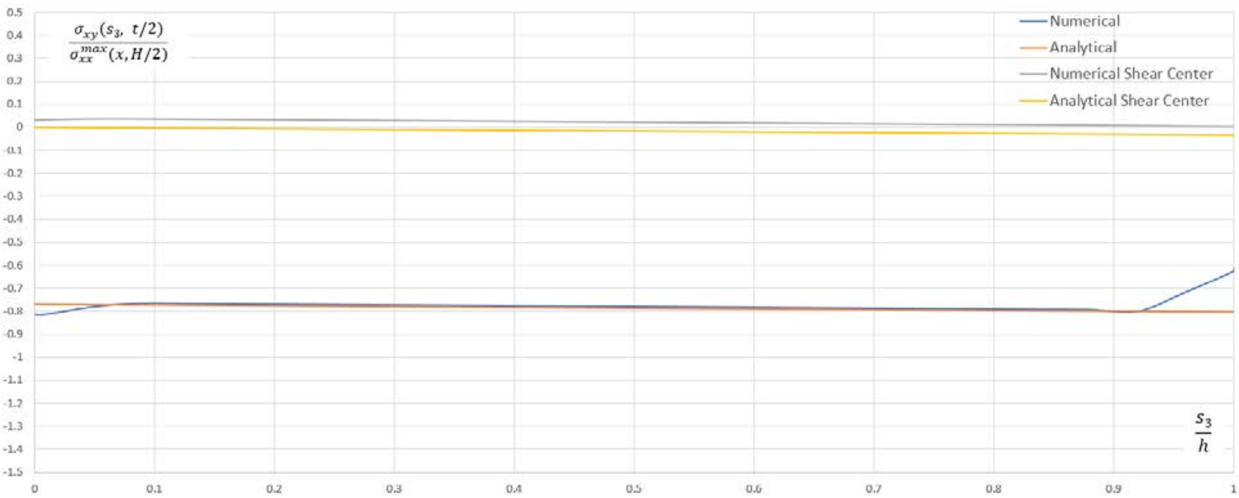

Figure 2.14: C-shell; normalized distribution of $\tau \equiv \sigma_{xy}(s_3, t/2)$ across the length of the bottom flange h. The numerical solution is compared to the analytical, the transverse load is applied at the *shear center*.

As it is shown in the figures (2.10), (2.11), and (2.12), if the transverse load is placed upon the shear center of the C-channel cross section (open section), the shear stresses τ diminish in magnitude across the beam. As a result, load placement upon the C-channel (open sections in general) is critical to ensure as low shear stresses τ as possible.

Following these series of graphs, down below the equivalent graphs for the A-shell cross section are presented.

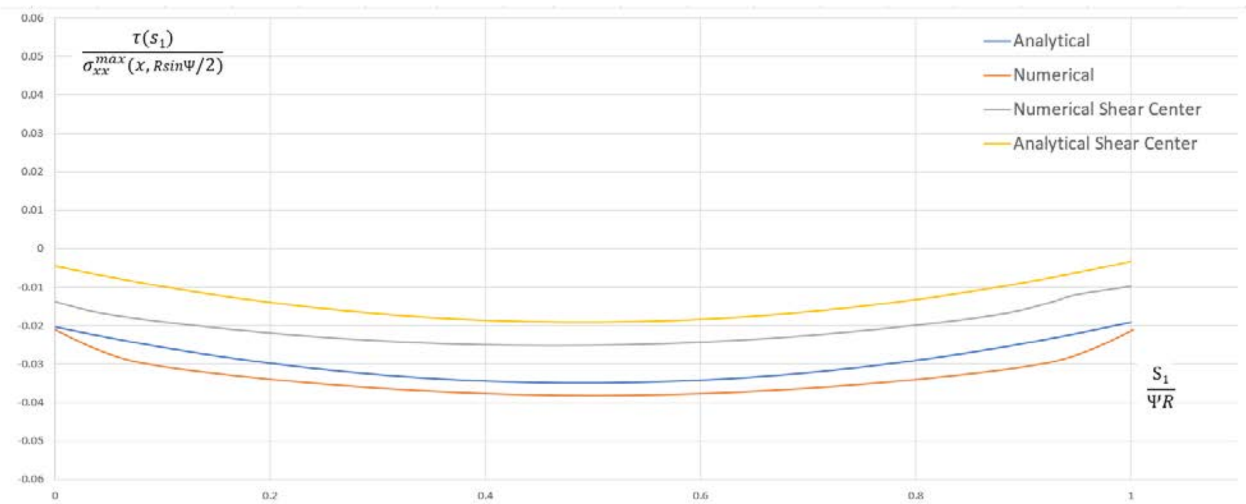

Figure 2.15: A-shell; normalized distribution of $\tau \equiv \tau(s_1)$ across the length of the curved section ABC of the aerofoil. The numerical solution is compared to the exact, the transverse load is applied at the *shear center*.

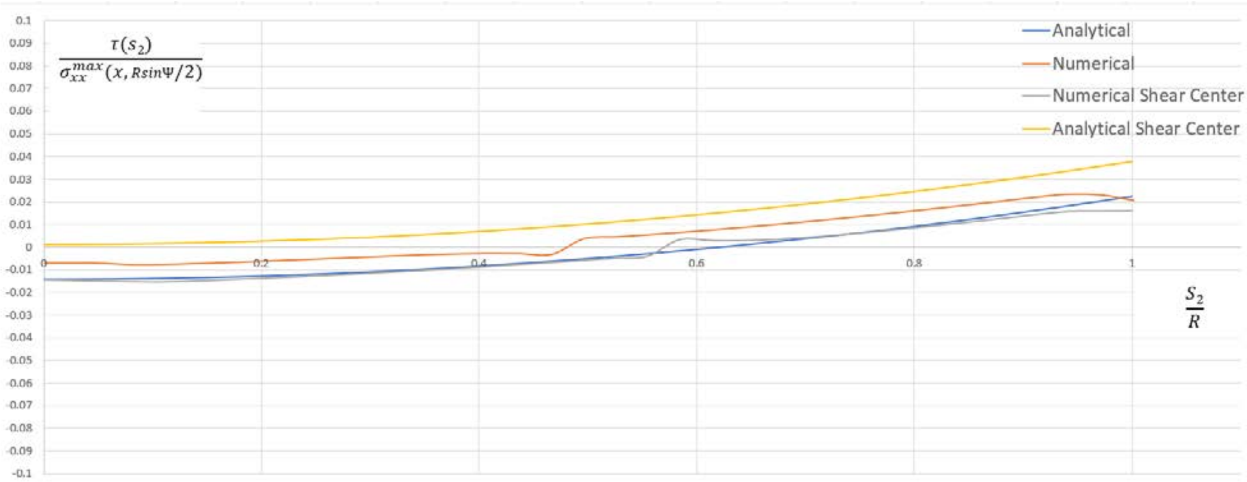

Figure 2.16: A-shell; normalized distribution of $\tau \equiv \tau(s_2)$ across the length of the upper side AO of the aerofoil. The numerical solution is compared to the analytical, the transverse load is applied at the *shear center*.

Figure 2.17: A-shell; normalized distribution of $\tau \equiv \tau(s_3)$ across the length of the lower side CO of the aerofoil. The numerical solution is compared to the analytical, the transverse load is applied at the *shear center*.

As it is shown in the figures (2.15), (2.16), and (2.17), in case a transverse load is placed upon the shear center of the A-shell cross section (closed section), the resultant shear stresses τ do not fluctuate as much compared to the C-channel cross section. Thus, it is proven that the A-shell (closed sections in general) is not as sensitive to load placement compared to an open section. With that being said, load placement is crucial in any beam application and should be examined thoroughly.

Discussion and Conclusions

The purpose of this thesis is to compare between an analytical approximate and a numerical solution, concerning the shear and normal stresses found in thin-walled prismatic beams, composed of a linear elastic isotropic material, utilizing both analytical and computational means.

Two prismatic cross sections were examined. First is a regular C-channel, which is considered an open cross section, meaning that the shape of the cross section does not contain any 'holes', and the mid-line C is physically disrupted at some point. The second beam examined is an A-shell prismatic beam. The A-shell resembles a rudimentary aerofoil and it is a closed cross section, so the mid-line remains uninterrupted all throughout the cross section. Both problems were approached analytically using the same triad of methods. That is, the Saint-Venant method for bending, the Technical Beam Theory, and Jourawsky's equation. The finite element method was implemented for the extraction of the numerical solution. Both beam models were generated and analyzed using the commercial FEA software ABAQUS. The make-up procedure for those two models was nearly identical. The boundary conditions implied on these models were a kinematic restriction on $x = 0$ beam end and a concentrated transverse load on the other $x = \ell$ beam end. After comparing those two results (analytical & numerical) the following observations have being made:

- The finite element method yield great results, given that the numerical model is well defined, and can be a powerful tool to aid in the analysis of such problems.
- The load placement is of grate importance since, slight load placement changes may increase shear stresses by a considerable margin and even exceeding normal stresses in magnitude. This observation holds true especially in the case of open sections, like the C-channel since, due to their geometric characteristics these cross sections are more susceptible to warping and deflecting.
- In the case of the C-channel, the classic kinematic restriction at the $x = \ell$ 'encastre', proved to be insufficient and did not yield accurate results, so an alternate restrictive method was employed.

Bibliography

[1] ABAQUS/Standard, Version 6.14, © Dassault Systémes, 2014

[2] ABAQUS, Analysis User's Manual, Version 6.14, © Dassault Systémes, 2014

[3] Aravas N., âĂŸMechanics of Materials âĂŞ Introduction to the Mechanics of Deformable Bodies and Linear ElasticityâĂŹ, Tziolas Publications, (2023).

[4] Aravas N., âĂŸMechanics of Materials Volume II: Elastic Beam AnalysisâĂŹ, University of Thes- saly Publications, (2008).